Xylem Surfactants Introduce a New Element to the Cohesion-Tension Theory[1][OPEN]

H. Jochen Schenk*, Susana Espino, David M. Romo, Neda Nima, Aissa Y.T. Do, Joseph M. Michaud, Brigitte Papahadjopoulos-Sternberg, Jinlong Yang, Yi Y. Zuo, Kathy Steppe, and Steven Jansen

Department of Biological Science, California State University, Fullerton, California 92831 (H.J.S., S.E., D.M.R., N.N., A.Y.T.D., J.M.M.); NanoAnalytical Laboratory, San Francisco, California 94118 (B.P.-S.); Department of Mechanical Engineering, University of Hawaii, Honolulu, Hawaii 96822 (J.Y., Y.Y.Z.); Laboratory of Plant Ecology, Department of Applied Ecology and Environmental Biology, Faculty of Bioscience Engineering, Ghent University, B–9000 Ghent, Belgium (K.S.); and Institute of Systematic Botany and Ecology, Ulm University, D-89081 Ulm, Germany (S.J.)

ORCID IDs: 0000-0001-6261-2780 (H.J.S.); 0000-0003-3307-9416 (D.M.R.); 0000-0002-3992-3238 (Y.Y.Z.); 0000-0002-4476-5334 (S.J.).

Vascular plants transport water under negative pressure without constantly creating gas bubbles that would disable their hydraulic systems. Attempts to replicate this feat in artificial systems almost invariably result in bubble formation, except under highly controlled conditions with pure water and only hydrophilic surfaces present. In theory, conditions in the xylem should favor bubble nucleation even more: there are millions of conduits with at least some hydrophobic surfaces, and xylem sap is saturated or sometimes supersaturated with atmospheric gas and may contain surface-active molecules that can lower surface tension. So how do plants transport water under negative pressure? Here, we show that angiosperm xylem contains abundant hydrophobic surfaces as well as insoluble lipid surfactants, including phospholipids, and proteins, a composition similar to pulmonary surfactants. Lipid surfactants were found in xylem sap and as nanoparticles under transmission electron microscopy in pores of intervessel pit membranes and deposited on vessel wall surfaces. Nanoparticles observed in xylem sap via nanoparticle-tracking analysis included surfactant-coated nanobubbles when examined by freeze-fracture electron microscopy. Based on their fracture behavior, this technique is able to distinguish between dense-core particles, liquid-filled, bilayer-coated vesicles/liposomes, and gas-filled bubbles. Xylem surfactants showed strong surface activity that reduces surface tension to low values when concentrated as they are in pit membrane pores. We hypothesize that xylem surfactants support water transport under negative pressure as explained by the cohesion-tension theory by coating hydrophobic surfaces and nanobubbles, thereby keeping the latter below the critical size at which bubbles would expand to form embolisms.

Vascular plants are the only organisms on Earth that transport water and nutrients under negative pressure. This negative pressure is hypothesized to be generated by the surface tension of capillary menisci in the nanopores of fibrous, cellulosic cell walls, mostly of the leaves, from which water evaporates into intercellular spaces and then moves as water vapor through stomata into the atmosphere, driven by strong, solar-powered humidity gradients. The cell walls are hydraulically connected to the rest of the plant's hydraulic system, which mainly consists of xylem tissue. Negative pressure created in evaporating walls drives sap flow in the xylem from roots to leaves due to strong cohesion between water molecules, which results in a water potential gradient (Askenasy, 1895; Dixon and Joly, 1895). This is the cohesion-tension theory of water transport (Pickard, 1981; Steudle, 2001). It would take at least -1 MPa of pressure in the leaves to move water up to the top of a 100-m-tall tree against gravity and more than that to overcome friction along the hydraulic pathway (Scholander et al., 1965; Koch et al., 2004).

While it is clear from physical principles and experimental microfluidic systems that evaporation from nanopores can create large negative pressures (Wheeler and Stroock, 2008; Vincent et al., 2012; Lamb et al., 2015; Lee et al., 2015; Chen et al., 2016), it remains unknown how plants can use this negative pressure to transport water through their xylem without constantly creating bubbles in the system (Jansen and Schenk, 2015), especially considering that xylem is highly complex, with many different surfaces and containing large amounts of gas (Gartner et al., 2004). The most successful attempt to mimic this process in an engineered system under

extremely controlled conditions managed to create several MPa of negative pressure in a single 3-cm-long hydrophilic microchannel (Wheeler and Stroock, 2008), but most other attempts have resulted in bubbles at much less negative pressures (Smith, 1994). Moreover, xylem sap has been found to be saturated or even supersaturated with atmospheric gas (Schenk et al., 2016), and gas supersaturation vastly increases the probability of bubble nucleation (Weathersby et al., 1982; Lubetkin, 2003), especially on rough hydrophobic surfaces (Ryan and Hemmingsen, 1998).

Bubbles in negative pressure systems most likely do not form through homogenous nucleation, because pure water has great tensile strength and can withstand negative pressures down to below −22 MPa under highly controlled stationary conditions (Dixon, 1914a; Briggs, 1950; Sedgewick and Trevena, 1976; Wheeler and Stroock, 2009; Chen et al., 2016). Bubbles are much more likely to form through heterogenous nucleation on particles or rough and hydrophobic surfaces (Crum, 1982; Wheeler and Stroock, 2009; Hedges and Whitelam, 2012; Rasmussen et al., 2012; Cho et al., 2015). The energy barrier E_{het} that has to be overcome to create a bubble through heterogenous nucleation is largely a function of surface tension (γ), which may be dynamic in the presence of surfactants and then dependent on surfactant concentrations, the contact angle between the liquid and solid phase (φ), and the liquid pressure (P_l); it is given by the equation:

$$E_{het} = \frac{16\pi\gamma^3}{3(P_l - P_v)^2} \times \left[(2 + 3\cos\varphi - \cos^3\varphi)/4\right] \quad (1)$$

(Blander and Katz, 1975; Khurana et al., 1998; Chen et al., 2016), where P_v is the water vapor pressure at the same chemical potential as the liquid at P_l. The first term on the right side of the equation is the energy barrier for homogenous nucleation, and the second term represents the effect of the contact angle on heterogenous nucleation. The likelihood of heterogenous nucleation as a function of liquid pressure depends further on the volume of the liquid phase and the area and geometry of the surface (Blander and Katz, 1975; Khurana et al., 1998; Wheeler and Stroock, 2009; Hedges and Whitelam, 2012). As a cubic term, surface tension (γ) has by far the strongest effect on the energy barrier of nucleation at a given liquid pressure. Contact angles above 0° (completely hydrophilic) reduce the energy barrier for heterogenous nucleation (e.g. by half for $\varphi = 90°$). Hydrophobic surfaces attract surface nanobubbles (Borkent et al., 2007; Craig, 2011; Lohse and Zhang, 2015), which can potentially expand under negative pressure to block entire conduits as embolisms.

Another source of bubble formation in xylem is so-called air seeding, by which bubbles enter through the nanopores of cellulosic pit membranes from a gas-filled into a sap-filled conduit (Tyree and Zimmermann, 2002; Schenk et al., 2015). The pressure difference ΔP_{bp}

required to force a bubble through a porous membrane is a function of the smallest radius R_p of the membrane's largest pore:

$$\Delta P_{bp} = \kappa\, 2\, \gamma\, \cos\varphi / R_p \quad (2)$$

(Schenk et al., 2015), with $\Delta P_{bp} = P_g + P_v - P_l$, where P_g is the gas pressure and κ is a dimensionless pore shape correction factor that can range between 0 and 1 (Emory, 1989; US EPA Office of Water, 2005). As for nucleation, surface tension (γ) and contact angle (φ) are important factors for bubble formation through air seeding, and both may be variable and depend on the nature and local concentration of surfactants. Although air seeding is commonly referred to as cavitation in the plant biology literature, it does not involve the formation of a cavitation void in sap and is simply the expansion of an existing bubble.

Bubble formation is such a serious problem for negative pressure systems that the existence of negative pressure in plant xylem has been questioned from the time it was first proposed until today (Schwendener, 1892; Bose, 1923; Peirce, 1936; Amin, 1982; Smith, 1994; Canny, 1995; Zimmermann et al., 2004; Laschimke et al., 2006). Yet, the circumstantial evidence for large negative pressure in plants, in some cases down to −8 MPa and below, is overwhelming (Angeles et al., 2004; Choat et al., 2012). This includes the observation that water is rapidly pulled into xylem when stems are cut and that it takes very large positive balancing pressures to force that water back up to the cut surface (Scholander et al., 1965). It also includes the fact that plant stems can be spun in centrifuges to create negative pressures artificially without forming embolisms until the sap in the stems approaches substantial negative pressure conditions (Holbrook et al., 1995; Pockman et al., 1995). Psychrometric chambers attached to and in equilibrium with functioning xylem also provide strong evidence for negative xylem pressure (Dixon and Tyree, 1984). Most importantly, the observation that plants in dry environments can take up water from soils with water potentials much lower than −2 MPa requires the existence of even lower water potentials in plants. However, all of this evidence is circumstantial. Direct measurements of strong negative pressure in individual xylem conduits using pressure probes proved to be impossible, because the insertion of a probe through the cell wall invariably creates leaks and nucleation sites (Wei et al., 2001). Despite all this evidence, the question that is at the root of the long-standing debate about the cohesion-tension theory remains valid: how can plants transport water under negative pressure?

The most widely accepted answer to that question has been that the very high surface tension of pure water prevents bubbles from entering through nanopores of cell walls, including pit membranes that separate xylem conduits (Tyree and Zimmermann, 2002). If this explanation were correct, if bubbles also could be kept out of the system during the formation of

functional xylem, and if surface nanobubbles were prevented by highly hydrophilic conduit walls, then it would appear to be possible to maintain a bubble-free xylem (Oertli, 1971). That explanation, however, is challenged by two facts: (1) xylem conduit walls do have some hydrophobic surfaces and cell wall irregularities (e.g. thickenings, warts, crevices, etc.; Laschimke, 1989; Kohonen, 2006; McCully et al., 2014), which could act as bubble nucleation sites; and (2) surface tension-lowering surfactants have been found in xylem sap (Christensen-Dalsgaard et al., 2011). In this study, we addressed these two apparent contradictions to the cohesion-tension theory by testing them for five plant species from five major angiosperm clades.

Of course, it is well known that xylem walls contain hydrophobic lignin, but there has been surprisingly little investigation of the surface properties of xylem conduits. Hydrophobic properties of xylem conduit walls have been shown by contact angles between menisci of sap or water and wall surfaces that deviate substantially from zero (Zwieniecki and Holbrook, 2000; Kohonen, 2006; Brodersen et al., 2010; McCully et al., 2014) and based on probes used to characterize wall surface properties (McCully et al., 2014). The evidence for xylem surfactants also should not have come as a surprise, because it is well known that xylem sap contains a large variety of molecules with potential surface-active properties, such as many different proteins (Buhtz et al., 2004; Dafoe and Constabel, 2009; Krishnan et al., 2011; Ligat et al., 2011; Zhang et al., 2015), glycoproteins (Iwai et al., 2003), and possibly phospholipids, which have been found in apoplastic fluid but not specifically in xylem sap to date (Gonorazky et al., 2012).

Recently, two hypotheses have been offered to explain these apparent challenges to the cohesion-tension theory. One of these proposes that xylem surfactants may not increase the likelihood of embolism formation but instead may coat bubbles and, due to low surface tension, substantially decrease the size of bubbles that form under negative pressure, thereby allowing them to remain smaller than the critical size at which pure gas bubbles become unstable under negative pressure (Schenk et al., 2015). The other theory proposes that xylem surfactants may coat hydrophobic surfaces and thereby render them hydrophilic (McCully et al., 2014). Both rely on the presence of surfactants in xylem, but currently there is direct evidence for xylem surfactants only for one species, *Populus tremuloides* (Christensen-Dalsgaard et al., 2011). More evidence for xylem surfactants is urgently needed before their possible functions in xylem can be evaluated.

This study was designed to test for hydrophobic vessel surfaces and surfactants in xylem of plant species from five major angiosperm clades. Xylem sap was tested for proteins and amphiphilic lipids, including phospholipids, as well as for evidence of surfactant-coated nanobubbles using nanoparticle-tracking analysis (Saveyn et al., 2010) and freeze-fracture electron microscopy (ff-EM; Papahadjopoulos-Sternberg, 2010). Surfactant properties of xylem sap residue were determined using constrained drop surfactometry (Valle et al., 2014). Locations of surfactant nanoparticles in xylem were examined via transmission electron microscopy (TEM).

RESULTS

Intervessel surfaces were probed with amphiphilic FM1-43 dye, which fluoresces yellow when excited with green light while binding to hydrophobic surfaces or to the hydrophobic portions of amphiphilic molecules. Vessel surfaces of all five angiosperm species showed distinct spatial patterns of fluorescence, reflecting different degrees of hydrophobicity (Fig. 1, A–E). Pit borders were generally more hydrophobic than other vessel surfaces, and the pit aperture rims were most brightly fluorescent in all species. All vessel wall surfaces were much more strongly fluorescent with FM1-43 than cell walls in adjacent phloem, which
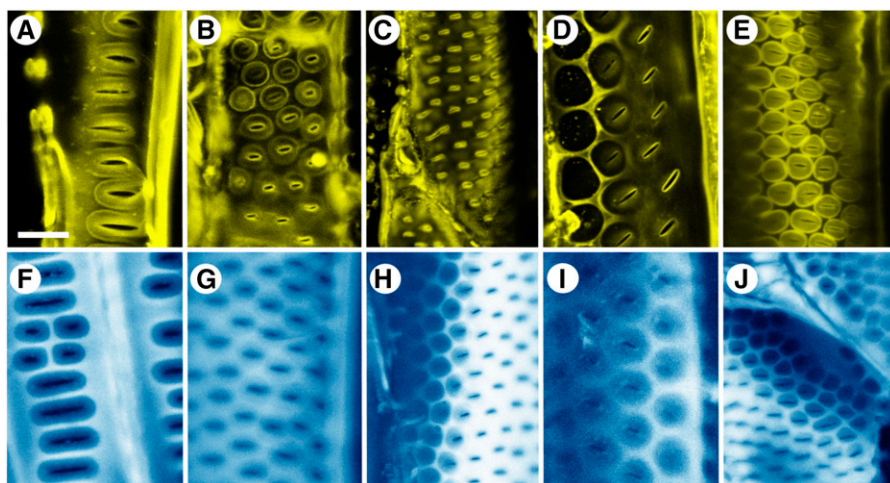

Figure 1. Intervessel walls with bordered pits and apertures in wood imaged by confocal microscopy with FM1-43 fluorescent dye to mark hydrophobic and amphiphilic surfaces (yellow color; A–E) and lignin autofluorescence (bright color, with darker blue indicating weakly lignified walls; F–J) under excitation at 405 nm. A and F, *Liriodendron tulipifera*. B and G, *Triadica sebifera*. C and H, *Geijera parviflora*. D and I, *Distictis buccinatoria*. E and J, *Encelia farinosa*. Bar = 10 μm for all images.

showed either very little or no fluorescence at all (data not shown), indicating that FM1-43 does not react with cellulose, as expected. The autofluorescence of lignin showed an almost exactly complementary pattern to FM1-43 (Fig. 1, F–J), suggesting that the hydrophobic surfaces detected by FM1-43 were not lignified. Most lignin was detected in vessel walls between pit borders, with pit borders and aperture rims showing less indication of lignins. The different fluorescence signals may come from different depths in the cell wall, but, taken together, these findings show that vessel walls of all species were clearly partially hydrophobic.

When probing lyophilized xylem sap residues for surfactants with fluorescent dyes, they tested positive for amphiphilic lipids (Fig. 2, A–D) and for proteins (Fig. 2, E–H). Small amounts of lipids and proteins were contributed to these samples from living cells at the cut

Figure 2. Evidence for amphiphilic molecules in xylem sap. Lyophilized xylem sap residue imaged in water by fluorescence microscopy from *T. sebifera* (A and B), *G. parviflora* (C and D), *D. buccinatoria* (E and F), and *E. farinosa* (G and H). A, C, E, and G, With FM 4-64; amphiphilic lipids in red. B, D, F, and H, With NanoOrange; proteins in yellow-orange. For controls, see Supplemental Figures S1 to S4. Bar = 100 μm for all images.

xylem surface, but the degree of contamination was very low, and control samples contained far fewer proteins and amphiphilic lipids (Supplemental Figs. S1–S4). A few samples from both xylem sap and contamination controls contained small traces of cellulose, presumably cell wall debris, but fluorescence of the cellulose stain Direct Red 23 was so low that the images were essentially black (data not shown). Traces of DNA from cut parenchyma cells were even lower, and hardly any fluorescence of xylem sap or contamination control samples was detected with SYTOX Green Dead Cell Stain (data not shown). Concentrations of choline-containing phospholipids in xylem sap (Table I) ranged from 0.5 μM L^{-1} for *D. buccinatoria* to 1.36 μM L^{-1} for *G. parviflora* (after correcting for cell contamination).

TEM revealed highly electron-transparent inter-conduit (including intervessel and intertracheid) pit membranes in samples of all five species studied that were only fixated with glutaraldehyde, which readily cross-links proteins (Fig. 3, A–E). This means that the pit membranes were difficult to detect due to their poor contrast within a bordered pit pair. Poststaining with uranyl acetate, which strongly stains proteins, followed by lead citrate, which binds to negatively charged groups such as hydroxyl and also membranes, improved the contrast of pit membranes slightly, although most remained rather transparent (Fig. 3, F–J). Poststaining showed minor differences across species and within a single TEM section (Fig. 3, H and I) and sometimes revealed dirt stain precipitates in nontissue areas (Fig. 3I) compared with samples without poststaining.

In contrast, samples fixated with glutaraldehyde and osmium tetroxide (OsO$_4$) showed dark, electron-dense nanoparticles associated with intervessel pit membranes (Fig. 3, K–S), pit borders (Fig. 3, K–O), at pit aperture rims (Fig. 3O), inner vessel walls (Fig. 3N), and pit canals (Fig. 3T). There was considerable variation in the electron density among the species studied but also within a single species (Fig. 3, N and S). The dark particles did not consist solely of polysaccharides or proteins, because neither of these molecules has high electron density under TEM. Because OsO$_4$ binds mainly to carbon double bonds in unsaturated fatty acid chains (Riemersma, 1968), the nanoparticles most likely consist of the same amphiphilic lipids detected in xylem sap (Fig. 2, A–D) and may be denatured aggregates that result when lipid micelles are subjected to the drying pretreatment that is necessary for TEM. At a high magnification, the particles appeared variable in shape, from linear and rod like to larger, snowflake and circular agglomerations (Fig. 3, P and Q). Most dark particles were smaller than 40 nm in diameter, but they also formed some larger, spherical aggregates embedded within intervessel pit membranes (Fig. 3, G and R) and were found on the outermost layers of a pit membrane (Fig. 3, K, M, P, and Q) and in a pit canal (Fig. 3T). Particles with an apparent dark coating clinging on the inner vessel wall were typically half-spherical and common in samples of all species (Fig. 3U). The
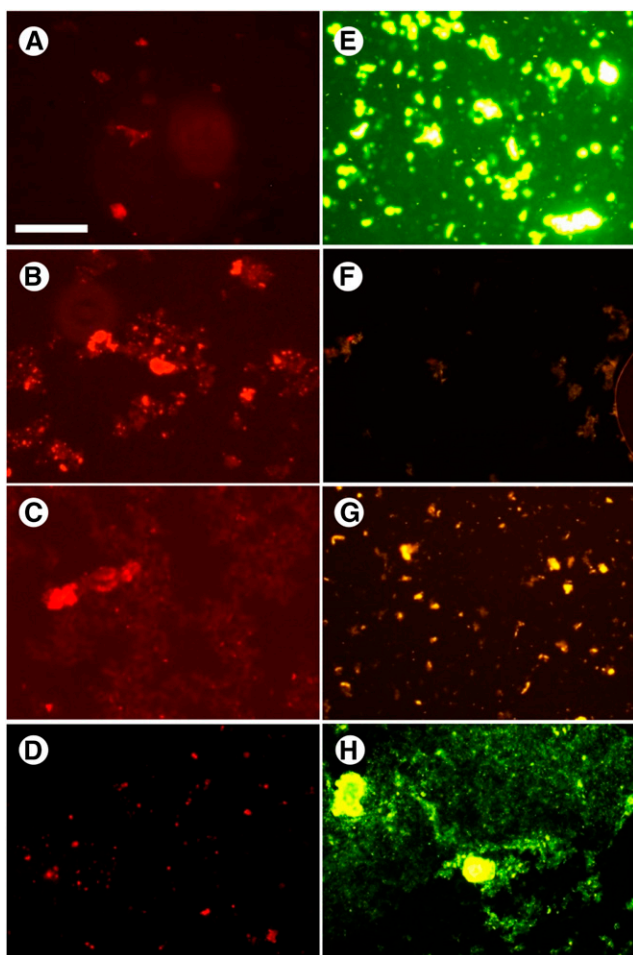
Table I. *Characteristics of extracted xylem sap, including concentrations of choline-containing phospholipids and nanoparticles in five angiosperm species*

Cell contamination controls were taken from the cleaned, cut xylem surface. Phospholipid concentrations were based on a phospholipid assay kit, while nanoparticle concentrations and diameter were measured with a NanoSight LM10-HS instrument. While most of the nanoparticles are likely to represent nanobubbles, the NanoSight instrument does not allow us to determine the exact nature of the particles measured. All data are means of four samples ± SE. Because nanobubble size distributions are skewed (Fig. 6B), diameter modes are listed in addition to means.

Species	Phospholipid Concentration		Nanoparticle Concentration		Nanoparticle Diameter			
	Mean		Mean		Mean		Mode	
	Sap	Control	Sap	Control	Sap	Control	Sap	Control
	$\mu M\ L^{-1}$		nL^{-1}		nm		nm	
L. tulipifera	0.85 ± 0.06	0.13 ± 0.13	136 ± 48	62 ± 17	278 ± 24	301 ± 33	218 ± 28	268 ± 43
T. sebifera	1.46 ± 0.23	0.08 ± 0.05	581 ± 46	31 ± 10	172 ± 19	235 ± 7	101 ± 29	160 ± 58
G. parviflora	1.45 ± 0.38	0.40 ± 0.18	454 ± 50	22 ± 11	236 ± 14	220 ± 58	180 ± 5	164 ± 15
D. buccinatoria	0.54 ± 0.11	0.04 ± 0.01	419 ± 138	88 ± 45	149 ± 24	126 ± 12	85 ± 13	82 ± 25
E. farinosa	1.92 ± 0.45	0.00 ± 0.01	467 ± 56	68 ± 10	158 ± 32	387 ± 66	93 ± 24	287 ± 23

outermost pit membrane layers in *D. buccinatoria* (Fig. 3, K and P) and *T. sebifera* (Fig. 3O) were more electron dense than the inner layers. The innermost layers of the pit membrane in *L. tulipifera* (Fig. 3, N and S) also were more electron transparent than the outermost layers. Poststaining of TEM samples that were fixated with glutaraldehyde and OsO_4 showed similar results as sections without poststaining, with little or no additional contrast enhancement of the pit membranes (data not shown).

The dark nanoparticles caused by OsO_4 staining only became visible in developing pit membranes after cell death (Fig. 4). In *L. tulipifera*, following the autolytic enzymatic removal of noncellulosic materials (Fig. 4, B and F), nanoparticles were arranged in a more or less regular, linear pattern but showed considerable variation in their density, suggesting a locally compact or loose microfibril arrangement (Fig. 4, C and D). Compression of the pit membrane in wood from the previous year's growth ring resulted in a thin pit membrane with distinctive dark layers on both sides of intervessel pit membranes (Fig. 4E). Dark OsO_4 staining also is visible on the walls of pit borders and vessel walls (Fig. 4, F–H, black double arrows) but is absent in a vessel element that has not fully differentiated yet (Fig. 4F, white arrows).

Vessel-associated parenchyma cells showed half-bordered pits with a dark, granular material, a so-called black cap (Schaffer and Wisniewski, 1989; Wisniewski et al., 1991), on the vessel side of many vessel-parenchyma pit membranes (Fig. 5), with many dark vesicles evident in the cytoplasm bordering the protective (or amorphous) layer on the parenchyma side (Fig. 5B). These vesicles also were observed across the plasma membrane while entering the first layers of the protective layer.

The surface tension of xylem surfactants was measured in vitro at much higher concentration than found in xylem sap, because surfactant nanoparticles are far more concentrated in pit membrane pores than in sap (Figs. 3, K–S, and 4), and pit membranes are typically the interface between the gas and liquid phases in xylem. Xylem surfactants were concentrated by lyophilizing sap from *D. buccinatoria* and *G. parviflora*, and their dynamic surface activity was determined via constrained drop surfactometry (Valle et al., 2015). Both possessed strong surface activity (Fig. 6) that reached surface tension values below 5 mJ m^{-2} when the adsorbed xylem surfactant films were contracted, similar to the behavior of pulmonary surfactants, which also consist of amphiphilic lipids and proteins (Zuo et al., 2008; Parra and Pérez-Gil, 2015). Lyophilized cell contamination residue in control samples did not show this surface tension-reducing capacity, except for a very weak effect at maximum surface contraction (Fig. 6).

Using nanoparticle-tracking analysis (Saveyn et al., 2010), substantial nanoparticle concentrations (between 136 and 581 nL^{-1}) below 300-nm radius were found in xylem sap of all five plant species tested (Fig. 7; Table I; Supplemental Movie S1), with diameter modes between 85 and 218 nm (Table I). Cell contamination controls contained much lower concentrations (between 22 and 88 nL^{-1}; Table I). Nanoparticle concentrations and size distributions in freshly extracted xylem sap were stable at least for several days when refrigerated (data not shown). The nanoparticles were found to be negatively charged, with ζ-potentials of −19.3 mV (SD 0.5) for *G. parviflora* and −36.1 mV (SD 2) for *D. buccinatoria*. These charges would provide moderate stability to the particles by causing nanoparticle repulsion and reducing the likelihood of coalescence and are in the range observed for nanobubbles in water (Ushikubo et al., 2010).

ff-EM of xylem sap of *G. parviflora* displayed coated nanobubbles ranging from 30 to 300 nm in diameter, with an average of 210 nm (Fig. 8). These nanobubbles show cross-fracture behavior revealing white inner gas volumes (Pt/C-free areas) and dark, Pt/C-decorated surfactant shells, which appear wrinkled and deflated. The surfactant shells are mostly chopped off from the original concave bubble depressions during the ff-EM process. They are observed partially still overlapping with the bubble depressions, as seen in Figure 8, B and C, or shifted away from the holes
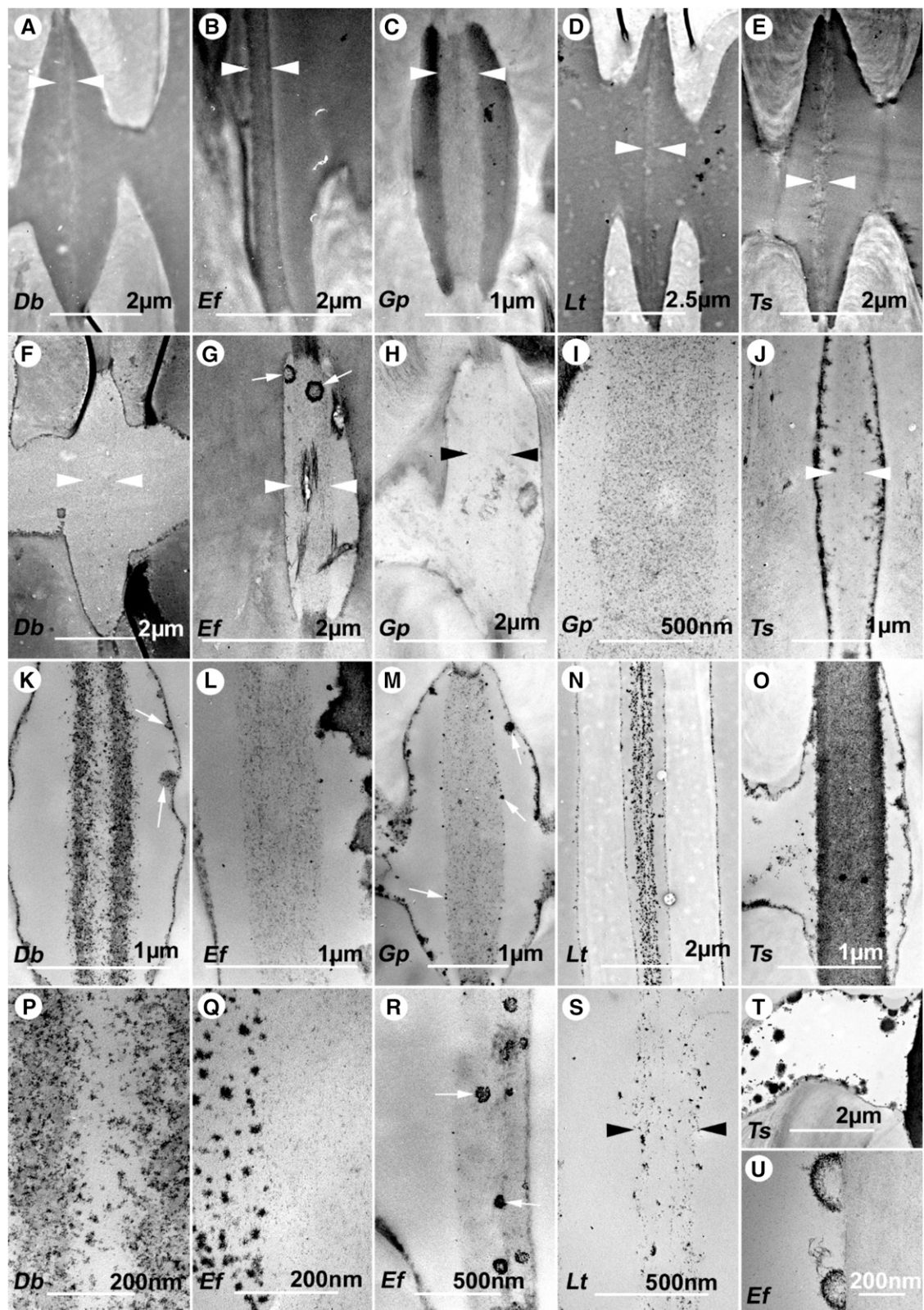
Figure 3. TEM images of transverse sections showing bordered, intervessel pits and their pit membranes after fixation with glutaraldehyde (A–E), fixation with glutaraldehyde and poststaining with uranyl acetate and lead citrate (F–J and U), and fixation with glutaraldehyde and OsO_4 (K–T). All images have an axial orientation. Triangles point to pit membranes that are electron transparent. No clear pit membrane can be seen after fixation with glutaraldehyde (A–E). Slightly improved contrast of the pit

(Fig. 8A). The lack of clear Pt shadowing in most bubble depressions clearly shows that the coats were still in the depressions during Pt shadowing and must have shifted afterward. At higher magnification, parts of surfactant shells, originally stabilizing the nanobubbles, also were detected as Pt/C-decorated rims at the periphery of the circular bubble cores (Fig. 8, B and C). The thickness of the basic surfactant shells, coating the bubbles, is about 2 nm, which is the resolution limit of this technique for periodical structures. Furthermore, a thicker but fussy layer is observed in addition to the basic surfactant monolayer. This unique glycocalyx-type fine structure is composed of fine white lines, stretching outward up to 120 to 130 nm in some cases (Fig. 8C). The coated nanobubbles reflect the same size range as found via nanoparticle-tracking analysis (Fig. 7B).

DISCUSSION

The findings of this study provide strong support both for the existence of hydrophobic surfaces in vessels and for substantial amounts of lipid-based surfactants in xylem of all five species tested. Xylem sap proteins also were detected in all five species, and some of these may have surface-active properties as well. The presence of surfactants in xylem was detected by no fewer than seven independent lines of inquiry, including fluorescent tracers in xylem and xylem sap, chemical assays of sap, TEM, ff-EM of xylem sap, surface-tension measurements of concentrated xylem sap, and nanoparticle-tracking analysis. These observations require a reevaluation of processes at interfaces between solid, liquid, and gas phases in xylem.

Hydrophobic Surfaces in Xylem Conduits

We found a variety of spatial patterns of hydrophobicity in vessels, with pit borders and pit aperture rims typically showing the strongest signals of the FM1-43 dye (Fig. 1, A–E) and surfaces between pits showing the strongest lignin autofluorescence (Fig. 1, F–J). In a previous study of vessels in maize (*Zea mays*) roots, McCully et al. (2014) made similar observations: pit borders and walls between pits stained with the lipophilic Rhodamine B and stained a greenish color with Toluidine Blue, indicating the presence of polyphenolic compounds (O'Brien et al., 1964; Feder and O'Brien, 1968). These areas between pit borders are most likely lignins. As in another study (Laschimke, 1989) and in ours, pit aperture rims and pit borders provided some of the strongest staining signals, providing evidence for both hydrophilic properties, staining with Ruthenium Red and the periodic acid Schiff reaction and staining pink with Toluidine Blue, and hydrophobic properties, staining strongly with Schiff reagent, which normally indicates the presence of aldehyde groups but also can be due to residual basic fuchsin in the Schiff reagent binding to phospholipids (Byrne, 1962; Adams and Bayliss, 1971). For any structures to stain with both hydrophilic and hydrophobic dyes clearly indicates an amphiphilic nature. The FM1-43 probe used in our study binds to all hydrophobic surfaces (we tested it for polystyrene; data not shown) but most strongly to amphiphilic molecules and, therefore, is commonly used as a membrane dye (Jelínková et al., 2010). In our study, FM1-43 provided the strongest signals at pit aperture rims (Fig. 1), and pit borders and aperture rims also were frequently found to be coated with dark nanoparticles under TEM (Fig. 4, E–H). Taken together with previous findings, the evidence points to the accumulation of amphiphilic substances at pit borders and apertures.

There have been various earlier observations of hydrophobic interior surfaces in xylem conduits based on a variety of methods, including microscopic stains (Laschimke, 1989; McCully et al., 2014), electron microscopy (Schneider et al., 1999; Wagner et al., 2000), experiments with organic solvents (Zimmermann et al., 2004; Westhoff et al., 2008; McCully et al., 2014), and observations of wetting angles in conduits (Zwieniecki and Holbrook, 2000; Kohonen, 2006; Brodersen et al., 2010; McCully et al., 2014). This body of evidence for plant species ranging from conifers to angiosperms, including monocots and eudicots, clearly shows that xylem conduit walls are partly hydrophobic. There is no question that hydrophobic surfaces have a much higher incidence of gas bubble nucleation than hydrophilic ones. For example, Brodersen et al. (2010) documented average contact angles in intact grapevine (*Vitis vinifera*) vessels of 94°, and such contact angles cut the energy barrier required for heterogenous nucleation roughly in half (Eq. 1). Heterogenous bubble nucleation would be even more likely when xylem sap is supersaturated with gas, which can happen at midday during rising temperatures (Schenk et al., 2016). Critics of the cohesion-tension theory have been correct when questioning whether water can be transported under negative pressure in hydrophobic conduits (Zimmermann et al., 2004). However, xylem sap is not pure water.

Evidence for Xylem Surfactants

The existence of hydrophobic surfaces in xylem conduits together with the massive evidence for water transport under negative pressure in plants (Scholander

---

Figure 3. (*Continued.*)
membranes is obtained after poststaining (F–J). Dark, electron-dense pit membranes occur after fixation with OsO_4, sometimes showing a darker staining at the outermost layers of the pit membranes (K, O, and P). Dark particles (arrows) can be seen on the outermost pit membrane layers (M and at left in Q) but also are associated with pit borders (K–O), pit canals (T), pit membranes (G and R), and the inner vessel wall (U). Species acronyms are given in the bottom left corner of each image: *Db, D. buccinatoria; Ef, E. farinosa; Gp, G. parviflora; Lt, L. tulipifera; Ts, T. sebifera.*
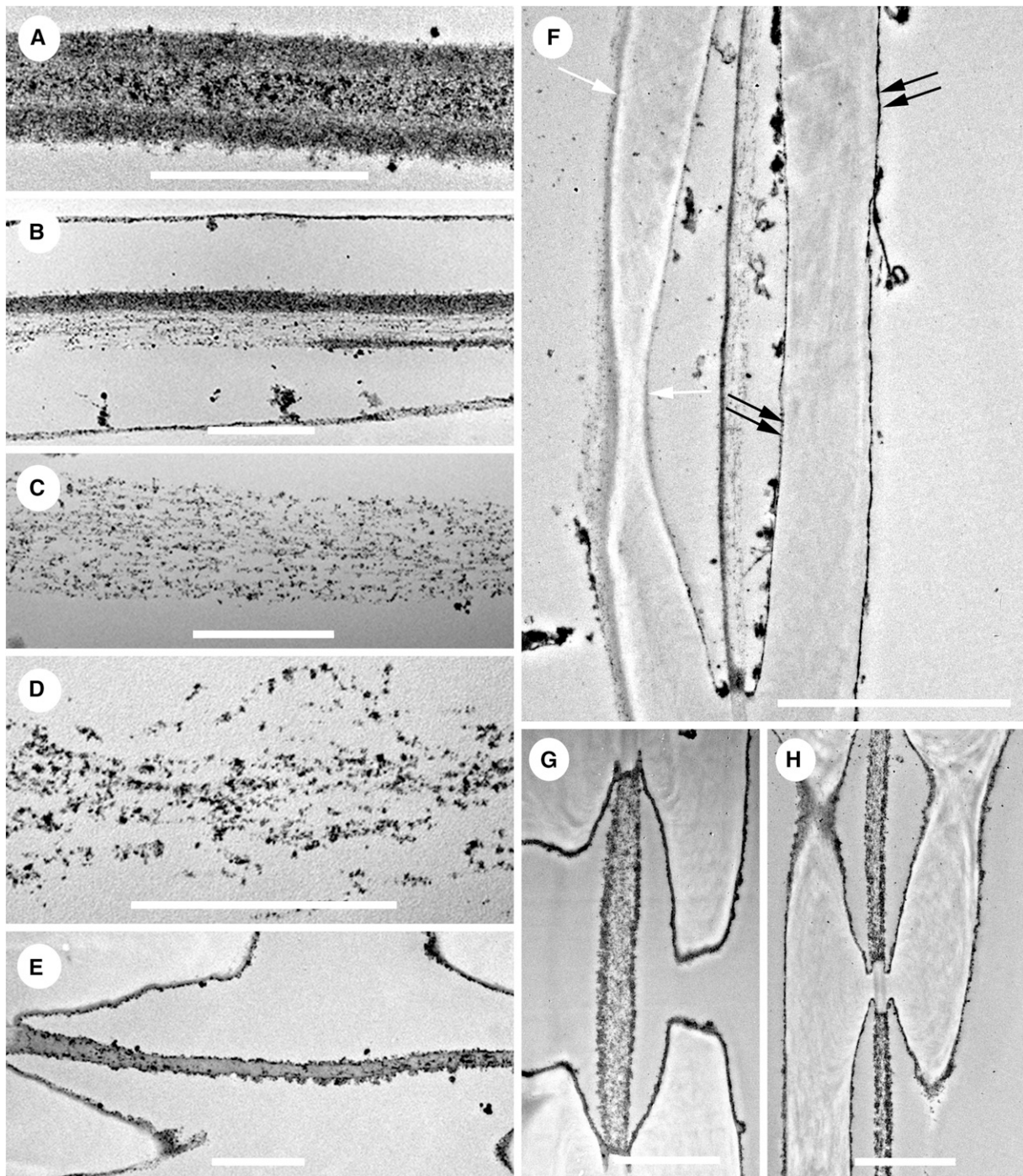
Figure 4. TEM images of transverse wood sections fixated with glutaraldehyde and OsO_4, showing various developmental stages of intervessel pit membranes. The cambium tissue (not shown) is at the top for A to E and on the left for F. The axial orientation is horizontal for A to E and vertical for F to H. A dark, electron-dense pit membrane is visible in living vessel elements, with the outermost layers darker than the inner layer (A). When the cell death process has started, autolytic enzymes gradually remove noncellulosic components, making the pit membrane more transparent at the side where cell differentiation is most developed (bottom side in B and right side in F). Pit membranes in fully developed vessel elements of the current year's growth ring include dark particles due to the reaction of OsO_4 with unsaturated lipids, suggesting a linear and loose arrangement of cellulose microfibrils, with a variable density and porosity (C and D). A pit membrane in the previous year's growth ring may shrink into a thin and more electron-dense structure, with a dark layer on the outermost sides (E). Dark OsO_4 staining also is visible on pit border walls and inner vessel walls (G and H, double black arrows in F) but is absent in a vessel element that has not fully differentiated yet (white arrows in F). A to F, *L. tulipifera*; G, *D. buccinatoria*; H, *T. sebifera*. Bars = 500 nm (A–D), 1 μm (E), and 2 μm (F–H).
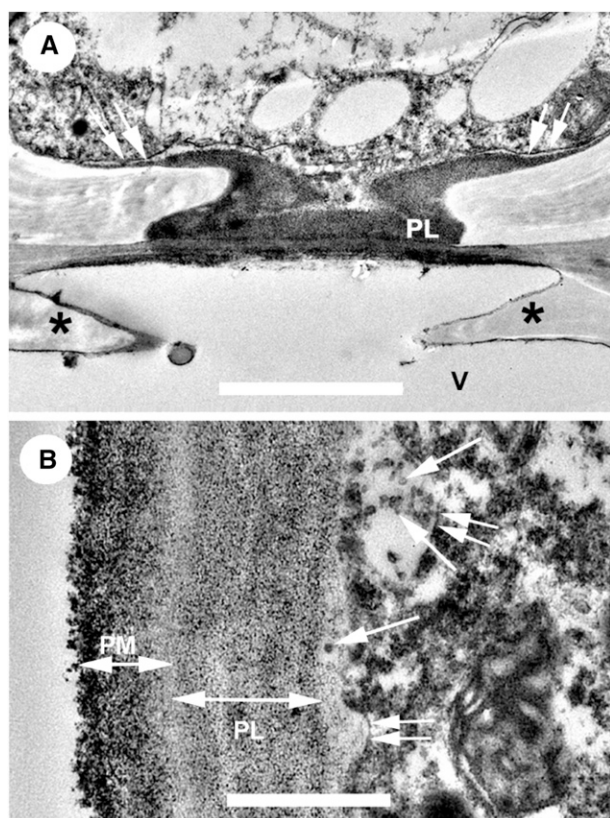
Figure 5. TEM images of transverse sections showing vessel-parenchyma pit membranes in wood of *L. tulipifera*. The pit membranes (PM) are dark and granular on the side of the vessel lumen (A) and in close contact with a dark protective layer (PL). Double arrows indicate the plasmalemma (A), and single arrows point to small vesicles that secrete substances from the parenchyma cell into the vessel lumen (B). Asterisks = pit borders. Bars = 2 μm (A) and 500 nm (B).

known functions in xylem sap. Our tests for cell wall and cell debris in xylem sap samples showed that the very thorough high-pressure cleaning of the cut xylem surface succeeded in removing almost all of such debris. Therefore, except for trace amounts, the surfactants found in xylem sap clearly originated from the contents of the vessels, not from other cells.

The finding of phospholipids in xylem sap is quite surprising, because they are very effective surfactants. Natural phospholipids are insoluble in water and form micelles at very low critical micelle concentrations that decrease with the length of carbon chains. For carbon chain lengths greater than 16 observed for phospholipids in the plant apoplast (Gonorazky et al., 2012), the critical micelle concentrations would be far below the concentrations observed by us in xylem sap (King and Marsh, 1987). The nanoparticles observed in xylem under TEM are mostly under 40 nm in diameter (Fig. 3, K–S), except when they are found in larger aggregations (Fig. 3, K, Q, R, and T), although their sizes and shapes can be affected by fixation and dehydration for TEM and, thus, may be different in intact xylem. The nanoparticles are clearly too large to pass through most angiosperm pit membranes, whose few largest pores are usually much below 100 nm in radius in the dried state (Jansen et al., 2009; Lens et al., 2011) and are probably much smaller than that when hydrated (Li et al., 2016). Therefore, nanoparticles carried in the transpiration stream would tend to accumulate on pit membrane surfaces and in their largest pores, as shown in Figures 3 and 4. The black particles seen in pit membranes and elsewhere in the xylem do not consist of pectins, as these are not black under TEM as lipids are after OsO_4 treatment and do not form particles in cell walls. Moreover, several recent studies have failed to detect pectins in angiosperm pit membranes, except in some cases at the outer margin, the so-called annulus (Plavcová and Hacke, 2011; Kim and Daniel, 2013; Dusotoit-Coucaud et al., 2014; Klepsch et al., 2016). The electron-dense particles also are clearly different from warts, which are outgrowths of the cell wall and mainly formed from lignin precursors (Liese, 2007).

Black nanoparticles in and on pit membranes and lining xylem conduit walls can be seen in TEM images from many previous studies of angiosperm xylem (Wagner et al., 2000; Schmitz et al., 2008; Jansen et al., 2009; Gortan et al., 2011; Lens et al., 2011; Scholz et al., 2013; Capron et al., 2014; Tixier et al., 2014; Li et al., 2016) as well as in ferns (Brodersen et al., 2014). Schmid (1965) and Schmid and Machado (1968) observed that pit membranes in young wood show a low scattering power, in certain instances to the point of almost complete transparency, while older pit membranes become electron dense again. This seasonal change in electron density was suggested to be either caused by an alteration of substances already present in the pit membrane or by secondary encrustation. The latter seems most likely, as substances from the xylem sap could be filtered out and deposited onto or within the pit membrane (Côté, 1958; Schmid, 1965; Wheeler,

et al., 1965; Dixon and Tyree, 1984; Holbrook et al., 1995; Pockman et al., 1995; Angeles et al., 2004; Choat et al., 2012) calls for an explanation. McCully et al. (2014) recently speculated that surfactants may provide that explanation, because amphiphilic surfactant molecules are capable of transforming a hydrophobic surface into a hydrophilic one. Our study provides strong support for that hypothesis, as black nanoparticles that reacted with OsO_4 and are likely to be remnants of lipid surfactant micelles were clinging to lumen-facing vessel surfaces and pit borders (Figs. 3, K, N, and O, and 4, E–H). The finding of significant concentrations of choline-containing phospholipids in xylem sap (Table I) is only the second published report for their presence in apoplastic fluid (Gonorazky et al., 2012) and, to our knowledge, the first specifically for xylem sap. Our study also adds to the abundant evidence for proteins in xylem sap (Fig. 2, D–H). Many proteins have amphiphilic properties, including so-called lipid transfer proteins that have been found in xylem sap of several species (Buhtz et al., 2004; Djordjevic et al., 2007; Dafoe and Constabel, 2009; Ligat et al., 2011) and have no
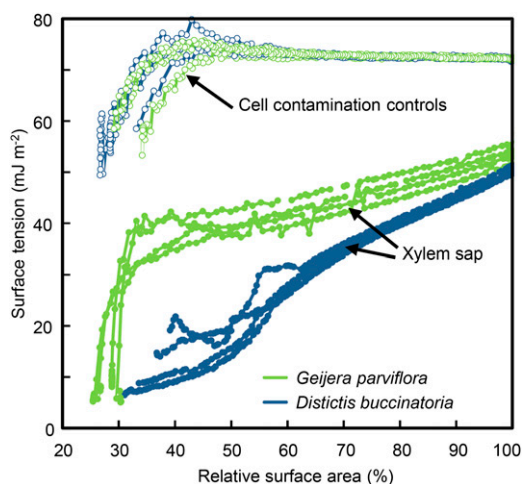
Figure 6. Surface tension of xylem sap residue and cell contamination control residue of *G. parviflora* and *D. buccinatoria* measured with constrained drop surfactometry as a function of drop surface area relative to the initial drop size, providing evidence for the concentration dependence of surface tension (i.e. dynamic surface tension). Note that the concentrations of surfactants in the residues are unknown and that the absolute surface tension values shown here may not be applicable to conditions in functioning xylem.

1981; Pesacreta et al., 2005). It would be fair to say that nanoparticles in intervessel pit membranes and on conduit walls have been hiding in plain sight for some time, although a few previous studies noted that they only appeared after OsO_4 fixation, indicating their lipid nature (Fineran, 1997; Westhoff et al., 2008). Wagner et al. (2000) observed a dark layer lining xylem conduits of the resurrection plant *Myrothamnus flabellifolia* (Myrothamnaceae) and speculated that it was composed of phospholipids, but they did not conduct a chemical analysis. Our findings suggest that this speculation was probably correct.

More evidence for the lipid nature of xylem surfactants comes from measurements of the area-dependent surface tension curves (Fig. 6), which are very similar to those found in pulmonary surfactants (Valle et al., 2014; Parra and Pérez-Gil, 2015). The composition of both may be similar, with phospholipids as the main components and proteins possibly playing a role in structuring the surfactant layers (Pérez-Gil, 2008). Both of these very different systems would represent adaptations for gas-liquid interfaces operating under widely fluctuating pressure conditions that require variable surface tension for optimal function. Constrained drop surfactometry provided evidence for variable surface activity of xylem sap residue, but the experimental behavior of concentrated xylem surfactants on small contracting and expanding droplets may differ from their behavior on gas-liquid nanointerfaces in xylem under negative pressure, so it remains unknown what the actual surface tension may be in functioning xylem.

ff-EM revealed surfactant coatings of xylem sap nanobubbles (Fig. 8). Although the thickness of the

basic surfactant shell coating the nanobubbles is about 2 nm (Fig. 8, B and C), which is consistent with a phospholipid monolayer, this measurement is very close to the resolution limit of the freeze-fracture technique (2 nm for periodical structures). Therefore, the coating layer also could consist of other amphiphilic molecules. As a matter of fact, lipid monolayer-stabilized microbubbles such as hydrophobic gas bubbles of the contrast agent Definity (Brancewicz et al., 2006) show concave fracture planes (shadow in front of the structures). Here, the fracture plane as the area of weakest forces runs along the interphase between the hydrophobic gas and the hydrophobic fatty acid tails of a phospholipid monolayer displaying concave fracture planes (Papahadjopoulos-Sternberg, 2010). Both fracture behaviors of gas-filled nano/microbubbles, cross fracture and concave fracture behavior, are very different from the fracture behavior of liquid-filled nano/microvesicles (liposomes or blebs). Liquid-filled vesicles are coated by bilayer membranes, which fracture along the hydrophobic center of their bilayers (area of weakest forces), revealing concave and convex fracture planes (Papahadjopoulos-Sternberg, 2010). Such a fracture behavior that is typical for bilayer-coated
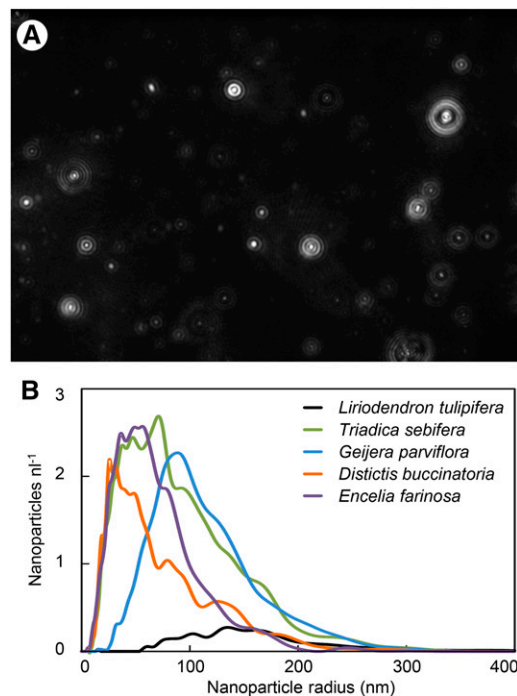

Figure 7. Nanoparticles in xylem sap. A, Nanoparticles in xylem sap of *G. parviflora*, imaged via nanoparticle-tracking analysis. Image size is $100 \times 80 \mu m$ (Supplemental Movie S1). Nanoparticle sizes are determined from particle velocity (Supplemental Movie S1), not particle size in the image. B, Nanoparticle concentrations and size distributions in xylem sap ($n = 4$, corrected for cell contamination) determined by nanoparticle-tracking analysis. For concentrations and mean and mode diameters for xylem sap samples and cell contamination controls, see Table I.
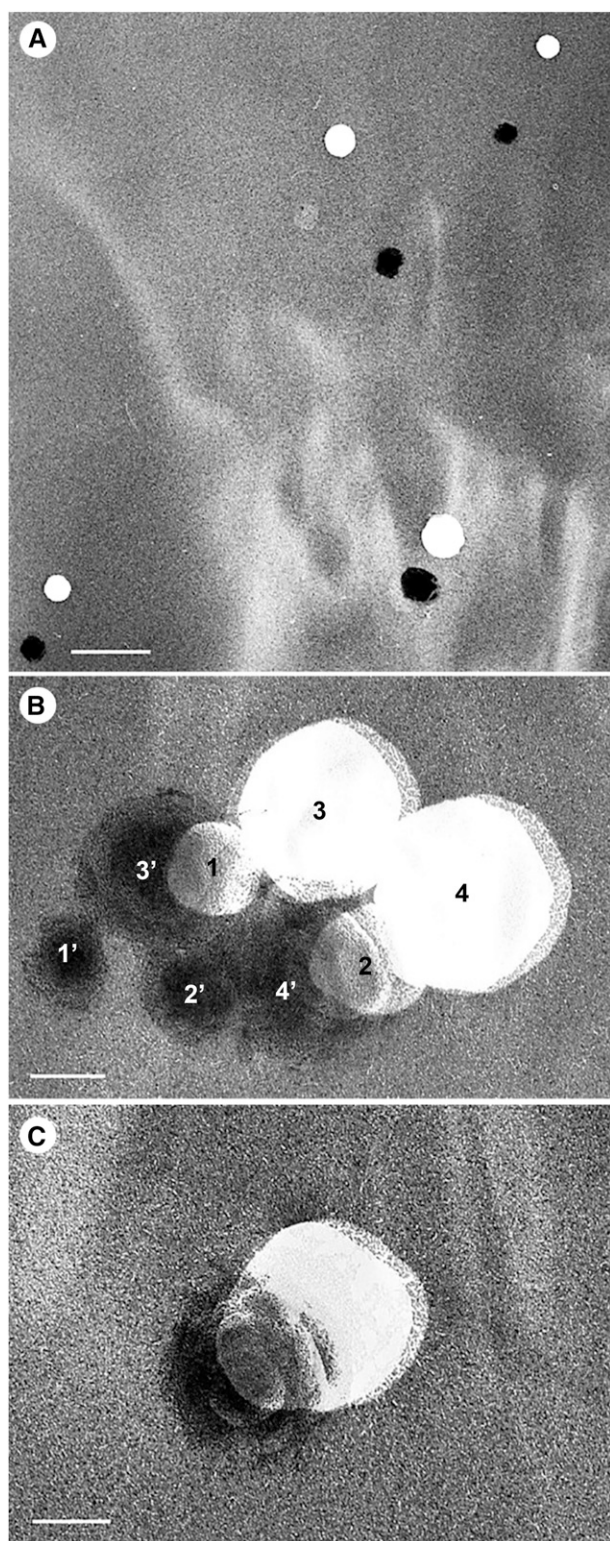
Figure 8. Freeze-fracture electron micrographs of surfactant monolayer-coated nanobubbles in *G. parviflora* xylem sap. Cross fractures display white gas bubble cores (Pt/C-free areas) and dark, Pt/C-decorated surfactant shells at the periphery of the bubble cores but also chopped off, shifted, and wrinkled during the ff-EM procedure (Supplemental Fig. S5). A, Surfactant coats (dark) shifted away from

vesicles was not observed at all in our study of xylem sap, resulting in the conclusion that many nanoparticles in sap are, in fact, coated nanobubbles.

Shifting of monolayer coats away from the original bubble holes after Pt shadowing (Fig. 8) also was observed in other ff-EM studies (Brancewicz et al., 2006; Uchida et al., 2016) and may be caused by the Pt-shadowed coat sliding off the convex shapes created by the former bubble holes in the carbon replica (Supplemental Fig. S5). Some wrinkling of surfactant shells, as observed in ff-EM images of xylem sap nanobubbles (Fig. 8), also is detected in smaller Definity microbubbles (Brancewicz et al., 2006) and lung surfactant- and lipid-covered microbubbles (Sirsi et al., 2009; Kwan and Borden, 2012). Contrary to this concave fracture behavior of lipid monolayer-stabilized microbubbles, the xylem sap nanobubbles visualized by ff-EM in this study show cross-fracture behavior revealing an inner gas volume, a basic surfactant shell, and, additionally, a thicker but fussy glycocalyx-type layer, possibly made of glycans, contributing to the stabilization of the nanobubbles. Freeze-fracture electron micrographs of polymer-stabilized microbubbles show similar cross-fracture behavior exposing a roughly 300-nm shell of polymerized polymer chains (B. Papahadjopoulos-Sternberg, unpublished data).

What Is the Origin and Chemistry of Xylem Surfactants?

The most likely source for phospholipids in xylem conduits are the conduit-associated parenchyma cells, which could be either ray or axial parenchyma cells (Fig. 5). Conduit-facing pit membrane surfaces of such cells often feature a coating of electron-dense material under TEM, the so-called black cap (Schaffer and Wisniewski, 1989; Wisniewski et al., 1991; Wisniewski and Davis, 1995; Rioux et al., 1998), and this cap may be the origin of the black nanoparticles elsewhere in the conduits. Further research will be required to test this hypothesis. Phospholipids also could remain in xylem conduits after cell death during conduit development (Fig. 4).

Seasonal comparisons of interconduit pit membranes show that electron-dense surfactants accumulate over time (Fig. 4, C–E), which also has been reported previously (Côté, 1958; Schmid, 1965). This seasonal change in electron density of the pit membrane combined with changes in pit membrane porosity and thickness may have substantial implications for the function of vessels at different ages and their vulnerability to embolism formation (Li et al., 2016). Increased vulnerability to embolism is well documented for older vessels in several plant species (Sperry et al., 1991; Melcher et al., 2003; Fukuda et al., 2015).

The chemistry of xylem surfactants will require much more research. Choline-containing phospholipids are

original bubble holes (white). Bar = 500 nm. B, Four bubbles (1–4) with surfactant coats (1′–4′) shifted away from holes. Bar = 100 nm. C, Bubble with surfactant coat on the periphery of the hole. Bar = 100 nm.

clearly a large component (Table I), but other amphiphilic lipids and proteins may be involved, including potentially glycoproteins. It is tempting to speculate that plant species adapted to tolerating low xylem water potentials in drought-prone environments will contain different amounts of xylem surfactants than plants from mesic environments, but the main difference may be in chemical composition and surface tension characteristics rather than in quantities.

Can Xylem Surfactants Be Reconciled with the Cohesion-Tension Theory?

Because seven independent lines of evidence support the conclusion that lipid-based surfactants occur in angiosperm xylem, the question arises how their existence can be compatible with the cohesion-tension theory (Askenasy, 1895; Dixon and Joly, 1895) and how they affect bubble formation under negative pressure (Schenk et al., 2015). The energy barrier required for bubble nucleation increases with surface tension cubed (Eq. 1; Blander and Katz, 1975; Khurana et al., 1998; Chen et al., 2016), which means that surface tension even slightly lower than that of pure water will increase the likelihood of nucleation enormously. Moreover, the pressure difference required for air seeding through pit membrane pores is a linear function of surface tension (Eq. 2). Accordingly, it has been axiomatic for a long time that surfactants would render xylem more vulnerable to air seeding and embolism formation (Christensen-Dalsgaard et al., 2011; Domec, 2011), and adding large amounts of artificial soluble surfactants does in fact have that effect in xylem (Sperry and Tyree, 1988; Cochard et al., 2009; Hölttä et al., 2012). Lipid-based, insoluble surfactants may act very differently, because their micelles concentrate in pit membrane pores and their surface tension is variable and area dependent (Fig. 6). The underlying mechanism for area-dependent surface tension is that insoluble surfactants (the so-called Langmuir film) are able to pack at the surface without collapse upon film compression. In contrast, soluble surfactant films (the so-called Gibbs film) usually collapse instantly upon compression (Kovalenko et al., 2014).

Predicting the behavior of this four-component system (gas, liquid, solid, and insoluble surfactant) under negative pressure is difficult, because there have been no previous studies of any such systems. The closest comparisons would be to drying soils (Or and Tuller, 2002, 2003; Sukop and Or, 2004; Moebius and Or, 2012), but soil studies have not considered insoluble surfactants. Given the lack of research on surfactant behavior in porous media under negative pressure, the following new theory is offered as a starting point for future research.

Surfactant-Coated Nanobubbles under Negative Pressure: A New Hypothesis

A coating of surfactants on a hydrophobic surface can reduce the contact angle to zero; therefore, the effects of contact angle, φ, on heterogenous nucleation (Eq. 1) and air seeding (Eq. 2) could be negligible in the presence of surfactants. However, surfactants also reduce surface tension, thereby vastly lowering the energy barrier required for nucleation, which is proportional to surface tension cubed (Eq. 1) and air seeding (Eq. 2). Surfactants in pit membranes (Fig. 4, B–H) would have the same effect of decreasing the energy barrier for bubble formation. Lipid surfactant micelles jammed tightly into pores (Figs. 3, K–S, and 4, C and D) would autoarrange into ordered layers at any gas-liquid interface, lower surface tension substantially, and greatly decrease the pressure difference required to force a gas bubble through the pore. Bubble expansion at the pore exit could potentially be limited by increasing the surface tension of stretched surfactant coats (Fig. 6). We note that the prediction by Schenk et al. (2015) that micelles would not penetrate into pit membrane pores most likely proved to be incorrect, as pit membranes are clearly clogged with lipid nanoparticles (Fig. 3, K–S). Because the surface tension of amphiphilic lipids is concentration dependent (Fig. 6), it is not possible to predict how low it may be in a given pore. To give an example for a possible effect of lipid surfactants on air seeding, a surface tension of 24 mJ m^{-2} (approximately the equilibrium tension for phospholipids; Lee et al., 2001), an effective contact angle of zero, and a pore shape correction factor κ of 0.5 for a fibrous medium (Meyra et al., 2007; Caupin et al., 2008; Schenk et al., 2015) would require only a pressure difference of 0.8 MPa to force a meniscus through a pore of 30-nm radius or of 0.4 MPa through a pore of 60-nm radius. These are probably realistic radii for the largest pores in hydrated pit membranes in vivo (Jansen et al., 2009; Lens et al., 2011) and normal xylem pressures under unstressed conditions. In addition, surfactants concentrated in nanopores may create much lower surface tension than assumed in this example (Fig. 6). In other words, where functioning xylem conduits are adjacent to gas-filled ones, bubbles are likely to pass through surfactant-clogged pit membrane pores all the time under normal xylem pressure conditions.

If bubbles could form so easily in the presence of surfactants either through heterogenous nucleation or air seeding, why would these bubbles not result in embolism under a much wider range of pressures than observed in plants? A possible answer to this question is that bubble formation will only result in an embolism if the resulting bubble expands beyond a critical size at which it becomes unstable. It is well known that bubbles can be stable under negative pressure as long as they remain below a critical size threshold (Blake, 1949; Oertli, 1971; Atchley, 1989; Schenk et al., 2015). That size threshold is determined by the balance of variables that cause the bubble to expand and those that cause it to contract (Atchley, 1989). Under negative liquid pressure, the expansion pressure, P_{exp}, is the sum of the internal gas (P_g) and water vapor pressure (P_v) minus the negative liquid pressure pulling from the outside (P_l):

$$P_{exp} = P_g + P_v - P_l \qquad (3)$$

The bubble compression pressure, P_{comp}, also known as the Laplace pressure, is caused by surface tension and bubble radius, R_b:

$$P_{comp} = 2\gamma/R_b \qquad (4)$$

The bubble is stable (assuming diffusion equilibrium between the internal gas concentration and the dissolved gas in the liquid) if $P_{exp} = P_{comp}$ and

$$P_g + P_v - P_l = 2\gamma/R_b \qquad (5)$$

Equation 5 is the well-known Laplace equation. It is sometimes overlooked, however, that bubbles may not be in Laplace equilibrium at all times. Under negative pressure conditions, if they are not in Laplace equilibrium, they will expand if $P_{exp} > P_{comp}$ and contract and dissolve if $P_{exp} < P_{comp}$ (Fig. 9). Thus, keeping bubbles below the critical radius where $P_{exp} = P_{comp}$ will allow them to shrink and dissolve. In aqueous environments, that critical radius under negative pressure is determined by the surface tension of pure water (72 mJ m^{-2}), which is higher than that of any surface-active substances that may be present. Thus, uncoated gas bubbles can attain higher stable radii at any negative liquid pressure than any surfactant-coated bubbles (Fig. 9). Conversely, stable surfactant-coated bubbles will be smaller under negative pressure than uncoated gas bubbles. This observation has important implications for nanobubbles in xylem. The processes involved are complicated by the diffusion of gas in and out of the bubbles (Louisnard and González-García, 2010), but for simplicity's sake, the following discussion assumes conditions of constant atmospheric pressure in the gas phase in equilibrium with dissolved gas in the liquid phase (Atchley, 1989).

An example for a critical bubble radius for a liquid pressure of −2 MPa (68 nm) is shown by point A on the black line in Figure 9. At this liquid pressure, any surfactant-free gas nanobubble smaller than this critical radius would have a surface tension of 72 mJ m^{-2}, be located on the black line to the left of point A, and therefore shrink and dissolve due to the high compression pressure. A surfactant-coated nanobubble at a hypothetical surface tension of 24 mJ m^{-2} would be in Laplace equilibrium at −2 MPa liquid pressure at about 23-nm radius (point B in Fig. 9). If this nanobubble became unstable, perhaps under slightly declining liquid pressure, and then stretched (Fig. 6), fractured, and eventually shed its surfactant coat, it could potentially expand by up to 3× its original radius and 27× its original volume before reaching the critical size. Of course, in reality, stretching (point B′ in Fig. 9) and shedding the surfactant coat (point C in Fig. 9) would create higher surface tensions than in the original bubble at point B, so nanobubbles of initial radius B would now be under a net compression pressure of
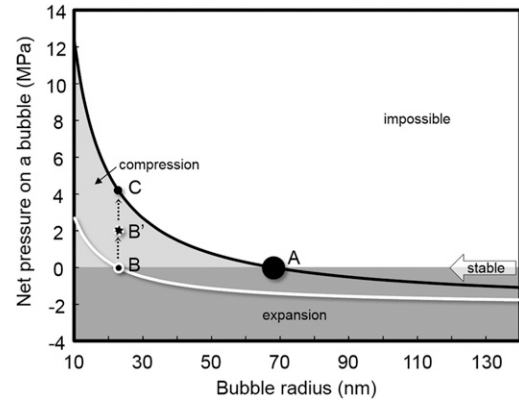

Figure 9. Net pressure (compression pressure − expansion pressure) acting on nanobubbles at a negative liquid pressure (P_l) of −2 MPa and surface tensions (γ; 24 [white line] and 72 [black line] mJ m^{-2}) for a typical lipid surfactant and pure water, respectively. Calculations assume a temperature of 20°C, atmospheric pressure in the gas phase at sea level, and constant surface tension. Net pressures were calculated based on Equations 3 to 5 as $P_{net} = P_{comp} - P_{exp} = 2\gamma/R_b - (P_g + P_v - P_l)$. A net pressure of zero (point A for pure water and point B for surfactant) indicates a stable nanobubble in Laplace equilibrium, negative values would lead to bubble expansion, while positive values would lead to bubble compression and dissolution. Points B′ and C are the net pressures experienced hypothetically in previously stable surfactant-coated nanobubbles of initial radius B after stretching (B′), fracturing, and shedding (C) their surfactant coats. Both would experience strong net compression pressure. For a full explanation of this figure, see text.

points B′ and C, respectively. Thus, they would not expand and instead would shrink and dissolve (Yount et al., 1977).

Clearly, stable or dissolving nanobubbles are not going to cause problems for plants, because they would not cause embolisms. But how about nanobubbles above the stability threshold size for a given liquid pressure (e.g. to the right of points A and B in Fig. 9 for high and low surface tensions, respectively)? Declining liquid pressure would quickly cause bubbles to be larger than the critical size and become unstable. On the one hand, changes in surfactant-coated nanobubble sizes would be accompanied by changes in area-dependent surface tension (Fig. 6), and this adjustment of surface tension with size can increase bubble stability (Atchley, 1989). Lipid surfactant coats also can buffer bubble size changes and reduce Ostwald ripening by slowing gas diffusion in and out of bubbles, especially when the coats collapse into dense structures (Yount et al., 1977; Duncan and Needham, 2004; Longo et al., 2009; Kwan and Borden, 2010, 2012; Fig. 8, B and C).

On the other hand, surfactant-coated nanobubbles are unlikely to be stable under rapidly declining liquid pressure, because this would increase the expansion pressure on the bubble (Eq. 3; Fig. 9), thereby increasing the bubble and lowering the Laplace pressure (Eq. 4). The resulting bubble expansion would eventually fracture the surfactant coat (Kwan and Borden, 2010,

2012), causing a sudden increase in surface tension of the newly exposed surfactant-free gas-liquid interface and Laplace pressure (e.g. from point B to B′ and further to C in Fig. 9), which then could compress and dissolve the bubble. As in pulmonary surfactants, proteins may play an important role in structuring the lipid layer and its expansion (Parra and Pérez-Gil, 2015) and possibly fracture. Fracture of the lipid shell also could lead to fragmentation into several smaller coated bubbles (Chomas et al., 2001; Bloch et al., 2004; Cox and Thomas, 2013). Bubbles minimize the surface energy-to-volume ratio, and surface tension is linearly related to surface energy (Yount, 1997; Winkel et al., 2004), so the surface energy-to-volume ratio of a surfactant-free gas bubble with the high surface tension of pure water is the same as that of 27 bubbles with one-third of the surface tension and one-third of the original bubble's radius. Thus, fracturing into coated nanobubbles would require less work than expanding the gas volume into a large irregularly shaped cavitation void and forming an embolism. Thus, both bubble dissolution and fragmentation into coated nanobubbles are probably energetically favored over bubble expansion and embolism formation.

Recent findings about the effects of surfactants under negative pressure provide experimental support for the rather counterintuitive hypothesis that surfactants could prevent embolism. A negative pressure system created using a 15.4-m-tall siphon proved to have reduced bubble formation when surfactants were added to the water (Vera et al., 2016). Even more intriguingly, Dixon (1914a, 1914b), one of the originators of the cohesion-tension theory, was the first to suggest that xylem sap may contain compounds that decrease the probability of embolus formation under negative pressure. He conducted experiments to measure the tensile strength of water and xylem sap under negative pressure and concluded that the findings "possibly indicate that sap is somewhat more stable under tension than pure water" (Dixon, 1914b). He speculated that "Possibly this very good cohesion possessed by unboiled sap is due to the presence of colloids in it" and suggested that the "fact that the presence of colloids leads to a large volume-contraction of the solvent may also increase the cohesion of the sap" (Dixon, 1914a). Remarkably, he observed that the formation of emboli was different in xylem sap than in water: "The click of rupture is not, in these cases, attended by the development of a single bubble becoming surrounded by a group of small visible bubbles, but, at the moment of rupture, a milky, semi-opaque region develops in the tube. This slowly rises, and clears away, as it turns into a mass of excessively minute bubbles. Here, apparently at the destruction of cohesion, countless numbers of minute ruptures have been simultaneously produced" (Dixon, 1914b). Dixon's experiments and those of Vera et al. (2016) both document a substantial decrease in the size of nucleating bubbles, in the latter case clearly an effect of the added surfactants. It is not much of a stretch to hypothesize that Dixon's

observations also were caused by the presence of xylem surfactants in the sap.

It is impossible to know exactly how large surfactant-coated nanobubbles are in intact xylem under negative pressure, because they are not under negative pressure once the sap is extracted. The vast majority of coated nanoparticles (presumed to be nanobubbles) in extracted xylem sap are below 200-nm radius (Fig. 7B), but bubbles may well coalesce or fragment during extraction or while under atmospheric pressure. Their surface tension also would change with changes in size (Fig. 6). Assuming that the observed nanoparticles are mostly nanobubbles (Fig. 8), it is clear that the surface tension of their surfactant coats in extracted sap must be close to zero, because these bubbles are fairly stable for days (i.e. in Laplace equilibrium) and, therefore, likely to be under internal atmospheric pressure. Solving Equation 4 for surface tension, γ, and entering the appropriate values for P_g, P_v, and P_l for atmospheric pressure conditions gives values very close to $\gamma = 0$ for all bubble radii (R_b) shown in Figure 7. The wrinkled appearance of the surfactant shell in Figure 8, B and C, also clearly shows the low surface tension of that shell, which looks almost exactly like other images of lipid-coated bubbles at very low surface tension (Pu et al., 2006; Kwan and Borden, 2012). The surface tension of surfactant-coated nanobubbles and their size distribution under negative pressure are completely unknown and could potentially be estimated using theoretical models.

With so much unknown about surfactant behavior under negative pressure, it is useful to focus on what is known. The findings of this study show that (1) lipid-based surfactants exist in xylem conduits, (2) they possess area-dependent surface tension, and (3) they accumulate in pit membrane pores, the most likely location of gas-liquid interfaces in xylem (Tyree and Zimmermann, 2002). On the other hand, there is massive evidence in the literature to show that xylem embolisms only form at low xylem pressures (Choat et al., 2012). Thus, xylem surfactants do not appear to increase the risk of embolism above that expected for the high surface tension conditions of pure water. We hypothesize that this apparent contradiction is explained by the fact that very small, surfactant-coated nanobubbles below the critical size for a given liquid pressure are safe (Fig. 9) and will not cause embolisms (Oertli, 1971). Given that xylem does not embolize that easily under normal pressure conditions, it is logical to hypothesize that lipid-based xylem surfactants function by reducing bubble sizes to below the critical radius (Jansen and Schenk, 2015; Schenk et al., 2015). That hypothesis remains to be tested in future research, using both experimental and modeling approaches.

It is important to note that surfactants cannot protect a hydraulic system completely against embolism formation. At pressure differences large enough to force a pure water meniscus through a pit membrane pore, the so-called air-seeding pressure, the production of small and safe surfactant-coated nanobubbles or coated surface nanobubbles would not be possible. Any liquid

pressure that could overcome the high surface tension of pure water in a pore also would create a very strong expansion pressure (P_{exp}) for the resulting bubbles that would be larger than the opposing Laplace pressure (P_{comp}; Eqs. 3–5). Thus surfactants cannot prevent classic air seeding and the resulting embolism formation, and this is consistent with observations of intact plant stems subjected to severe drought stress (Brodersen et al., 2013; Jansen and Schenk, 2015; Knipfer et al., 2015; Torres-Ruiz et al., 2015).

CONCLUSION

Xylem surfactants may provide an answer to the 120-year-old question of how vascular plants can transport water under negative pressure (Schwendener, 1892; Strasburger, 1893; Askenasy, 1895; Dixon and Joly, 1895; Greenidge, 1954; Smith, 1994), even in a hydraulic system that is full of gas-filled spaces, hydrophobic surfaces, and saturated or supersaturated with gas (Schenk et al., 2016). They also may allow safe gas removal from embolized conduits in the shape of surfactant-coated nanobubbles that quickly dissolve without causing embolism. Because xylem surfactants were observed across the phylogenetic tree of angiosperms, it seems likely that they are a universal feature of plant xylem and most likely will be found in gymnosperms and ferns as well. The challenge for future research will be to identify the origin, chemical composition, and physical characteristics of xylem surfactants in different plants as a function of xylem development, season, temperature, and drought. Most likely, the biology of xylem surfactants will be as complex as that of pulmonary surfactants (Parra and Pérez-Gil, 2015) and under some control by the living cells in the xylem. Wood is not a dead tissue, and living cells are likely to play an active role in maintaining its function for water transport. The presence of surfactant in xylem adds a new supporting element to the cohesion-tension theory and also addresses long-standing observations and arguments from critics of that theory, thus providing a way forward to resolve one of the longest enduring debates in plant biology (Schwendener, 1892; Bose, 1923; Peirce, 1936; Smith, 1994; Canny, 1995; Angeles et al., 2004; Zimmermann et al., 2004).

MATERIALS AND METHODS

Study Species

Study species were selected to include woody plants from five major angiosperm clades (APG III, 2009) and different growth forms: *Liriodendron tulipifera* (winter-deciduous tree; Magnoliaceae, Magnoliales, magnoliids clade), *Triadica sebifera* (syn. *Sapium sebiferum*; winter-deciduous tree; Euphorbiaceae, Malpighiales, fabids clade), *Geijera parviflora* (evergreen tree; Rutaceae, Sapindales, malvids clade), *Distictis buccinatoria* (evergreen liana; Bignoniaceae, Lamiales, lamiids clade), and *Encelia farinosa* (drought-deciduous desert shrub; Asteraceae, Asterales, campanulids clade). All experiments and measurements were conducted with *G. parviflora* and *D. buccinatoria*, with a subset of measurements conducted for the other species. All grew in the Fullerton Arboretum

or on the California State University campus in Fullerton, California. Some investigations using TEM also were done with specimens of *L. tulipifera* growing in the botanic garden at Ulm University.

Confocal Microscopy of Xylem Vessels

To detect hydrophobic surfaces on lumen-facing vessel walls, tangential sections of xylem in small woody stem pieces (4–10 mm in length and width) were imaged under water with laser scanning confocal microscopy (model TCS SP2; Leica) with a 63× objective. Lignin autofluorescence emission of blue light between 430 and 470 nm was examined under excitation with a near-UV 405-nm laser (Donaldson and Radotic, 2013). To detect other hydrophobic surfaces, stem pieces were soaked in water-soluble amphiphilic FM1-43 dye (Molecular Probes, Life Technologies) at 5 μg mL^{-1} concentration. Lasers at 476 and 488 nm were used for excitation, and emission was set to a window of 578 to 618 nm. No autofluorescence of xylem was ever detected with the 476- and 488-nm excitation settings, and all control samples without FM1-43 dye were always completely black.

Xylem Sap Extraction

Branches were cut from the plants at a length exceeding the longest vessel for each species, which had been measured previously via air injection (Greenidge, 1952). Stems were transported immediately to the laboratory, submerged completely under water, and cut again under water, with the final cuts made with a fresh razor blade. The bark was removed (from the distal stem end for positive pressure extraction and the proximal end for vacuum extraction; see below) for about 0.5-cm length to expose the xylem cylinder. The cut surface was thoroughly cleaned with deionized water using a high-pressure dental flosser (WP-100 Ultra Water Flosser; Waterpik) for 2 min to remove cell debris and cytoplasmic content from the surface. Latex tubing was mounted tightly over the exposed xylem cylinder, and Tygon tubing was inserted over it for collecting the cell contamination control and sap samples. After mounting the tubing, the xylem surface was cleaned again using the dental flosser for 2 min. A control sample to determine the amount of contamination from living cell remnants from the cleaned, cut surface was taken by pipetting 1 mL of nanopure water onto the cut surface and leaving it there for 1 min. It was then pipetted off and was included in all chemical and physical analyses. All samples and controls were immediately refrigerated after extraction. For some chemical analyses, freshly extracted xylem sap and cell contamination controls were flash frozen in liquid nitrogen immediately after extraction, lyophilized in a freeze drier (FreeZone 1 Liter Benchtop Freeze Dry System) for 24 h, and afterward stored in a freezer until they could be analyzed. Freeze drying was found to be useful for storing xylem surfactants for a long time and to increase xylem surfactant concentration.

Positive Pressure Extraction

Xylem sap was extracted under positive pressure for all measurements that required intact nanobubbles, including nanoparticle-tracking analyses, ζ-potential measurements, and ff-EM. The proximal end of the stem was inserted into a pressure chamber (model 1000; PMS Instruments) through the chamber lid gasket into a beaker filled with pushing liquid (0.5% aqueous acid fuchsin solution) inside the pressure chamber. Pressure was applied with compressed nitrogen at between 0.05 and 0.3 MPa. For most experiments, no more than 1 mL of sap was extracted, because extraction of larger volumes typically yielded lower concentrations of nanoparticles and surfactants, presumably because these do not pass through pit membranes. Sap collection was stopped immediately at the sign of pink acid fuchsin dye emerging from the xylem surface. Xylem sap was collected using a fresh Pasteur pipette and transferred to 1.5-mL Eppendorf tubes.

Vacuum Extraction

Sap extraction under vacuum typically yields more sap than positive pressure extraction, which is why sap for chemical and surface tension analyses was extracted via the vacuum method. After collecting the cell contamination control, the Tygon tubing was removed from the proximal branch, leaving the latex tubing around the xylem cylinder, and this was then fitted into Tygon tubing connected to a pipette tip, and facing downward, inserted into a vacuum flask. Sap dripping from the pipette tip was collected with a test tube inside the flask. The flask was subjected to laboratory vacuum for 30 s. The distal end of the branch was then cut back by about 4 cm, followed by successive 2-cm cuts, which

were made to all the side branches of the stem until sap was observed dripping into the test tube. Once dripping sap was observed, further 2-cm cuts were made every 1 min to allow for slow, continuous removal of xylem sap, until the final cut reached the Tygon tubing at the vacuum flask. Xylem sap was collected from the test tube using a fresh Pasteur pipette.

Chemistry of Xylem Sap

Quantification of Choline-Containing Phospholipids

A phospholipid assay kit (Sigma-Aldrich) was used in fluorimetric mode. The kit uses phospholipase D enzyme to cleave choline from choline-containing phospholipids and then uses choline oxidase to convert choline (+oxygen) into betaine aldehyde and hydrogen peroxide (H_2O_2). The H_2O_2 is then detected using the fluorescence of an H_2O_2-specific dye and compared with a standard curve created with a phosphatidylcholine standard. Previous experiments had established that all free choline in xylem sap resulted from native phospholipase D activity as part of a common wounding response (Wang et al., 2000; Bargmann et al., 2009), which could be inhibited completely by the addition of $CuCl_2$ (data not shown; Abousalham et al., 1995). Therefore, all choline detected by the assay kit was concluded to originate from choline-containing phospholipids. Because of the low concentration of phospholipids in xylem sap, samples ($n = 4$) and their contamination controls were concentrated by a factor of $10\times$ from the originally collected volume of 1 mL by suspending lyophilized residue from vacuum-extracted xylem sap in 0.1 mL of nanopure water. After treatment with the assay kit, fluorescence (excitation = 530 nm and emission = 585 nm) was measured on black 96-well plates (Corning) using a microplate reader (SpectraMax M3; Molecular Devices).

Fluorescence Microscopy of Xylem Sap Residue

Lyophilized residue from xylem sap ($n = 4$) and their cell contamination controls was examined using fluorescence microscopy (Olympus BX41 Laboratory Microscope; Olympus America) to test for the presence of amphiphilic lipids, proteins, cellulose, and DNA, the latter two to account for cell and cell wall debris from the cut wood surface. Lyophilized residue was suspended with 10 μL of nanopure water, then that suspension was divided into two 5-μL portions that were pipetted separately onto a microscope slide. One portion received 5 μL of a fluorescent dye solution (see below), while the other received an addition of 5 μL of nanopure water to act as the control without dye. To test for cellulose from cell walls, we used Direct Red 23 (item no. 212490; Sigma-Aldrich), also known as Pontamine Fast Scarlet 4B, which is a cellulose-specific stain that fluoresced red following green excitation (Thomas et al., 2013). To test for cytoplasmic contents from living cells that may have remained on the xylem surface even after the thorough cleaning, we used SYTOX Green Dead Cell Stain (item no. S34860; Fisher Scientific), which is a cell-impermeant DNA-binding dye. Water-soluble FM4-64 dye (Molecular Probes, Life Technologies) in 5 μg mL^{-1} concentration was used to test for the presence of amphiphilic lipids (Jelínková et al., 2010). Water-soluble NanoOrange dye (Molecular Probes, Life Technologies) as $1\times$ working solution was used to test for the presence of proteins. Images were taken at $20\times$ magnification under phase-contrast, bright-field, and fluorescence modes. Samples treated with Direct Red 23, SYTOX Green Dead Cell Stain, and FM4-64 and corresponding samples without those dyes were examined under excitation with green light, emitting red light when bound to cellulose, DNA, and amphiphilic lipids, respectively. Samples treated with NanoOrange were examined under excitation with blue light and emitted yellow-orange light when bound to proteins.

TEM

Fresh wood samples were collected in December 2014, wrapped in wet tissue, and express shipped to the Jansen laboratory in Ulm, Germany, for TEM. Small sectioning blocks were given two different treatments: (1) fixation with a solution containing 2.5% glutaraldehyde, 1% saccharose, and 0.1 M phosphate buffer at pH 7.3; and (2) fixation with glutaraldehyde first and then postfixation with a 2% aqueous OsO_4 solution for 2 h at room temperature. The samples were then dehydrated through a gradual ethanol series and embedded in Epon resin. Moreover, samples that were treated with glutaraldehyde only were observed with and without poststaining of TEM grids with aqueous uranyl acetate and lead citrate to test the potential staining effect on vessel-vessel pit membranes (Ellis, 2014). The duration of the staining was 5 min for uranyl acetate and 1 min for lead citrate. Transverse semithin sections were cut with an ultramicrotome (Leica

Ultracut UCT; Leica Microsystems), stained with 0.5% Toluidine Blue in 0.1 M phosphate buffer, and mounted on microscope slides using Eukitt. Ultra-thin sections between 60 and 90 nm were mounted on copper grids (Athena; Plano) and observed with a JEM-1210 TEM device (JEOL) at 120 kV. Digital images were taken using a MegaView III camera (Soft Imaging System).

Surfactometry

The dynamic surface tension of xylem sap was determined with a constrained drop surfactometer (CDS; BioSurface Instruments; Goetzman et al., 2014; Valle et al., 2015). The CDS uses the air-water interface of a sessile drop (approximately 3 mm in diameter, approximately 0.1 cm^2 in surface area, and approximately 10 μL in volume) to accommodate the adsorbed surfactant films and is well suited for assessing very scarce surfactant samples. The sessile droplet in the CDS is constrained on a carefully machined hydrophilic drop holder with a knife-sharp edge that prevents the droplet from spreading even at very low surface tensions. The surfactant film can be compressed by withdrawing the subphase liquid from the droplet using a motorized syringe. Surface tension is determined photographically from the shape of the droplet using axisymmetric drop shape analysis (ADSA; Zuo et al., 2004a, 2004b, 2007). ADSA measures the surface tension accurately and remotely, thus minimizing potential sample contamination and facilitating undisturbed drop oscillation.

For surfactometry, 10 mL of xylem sap was extracted from both *D. buccinatoria* and *G. parviflora* via the vacuum extraction method. Ten 1-mL samples of cell contamination controls also were collected from freshly cleaned xylem surfaces from the same stems and combined into a 10-mL sample (see xylem sap extraction methods above). Sap and controls were lyophilized to obtain residues, including any surfactants. Residues were shipped to the Zuo laboratory at the University of Hawaii in 1.5-mL Eppendorf tubes. There, 10 μL of Millipore water was added to each residue sample, including cell contamination controls, and any residue clinging to walls was scraped off. The sample was then subjected to 2 min of ultrasonic treatment for mixing and another 1 min of ultrasonic treatment immediately before every measurement in the CDS.

To use the CDS for lyophilized xylem sap residue, a pure water droplet of approximately 10 μL was formed on the CDS drop holder. A xylem sap residue sample of approximately 1 μL was spread at the drop surface and allowed 5 min to reach equilibrium. Subsequently, the surfactant film was compressed at a rate of approximately 20% relative area per second to concentrate the surfactant molecules at the drop surface. All measurements were conducted at room temperature of 20°C $\pm$ 1°C. Surface tension, surface area, and drop volume were determined with ADSA (Zuo et al., 2004a, 2004b, 2007). Data were expressed as means $\pm$ SE ($n > 3$ unless indicated otherwise). Group differences were analyzed by one-way ANOVA. $P < 0.05$ was considered statistically significant.

Nanoparticle Analysis

Nanoparticle-Tracking Analysis

Concentrations and size distributions of nanoparticles in freshly expressed xylem sap (using positive pressure extraction) and their cell contamination controls (both $n = 4$) were determined in 1-mL samples using a NanoSight LM10-HS instrument with a 405-nm laser connected to a syringe pump (Malvern Instruments) and visualized in videos (Saveyn et al., 2010). The concentration and size distribution of nanobubbles were determined using NanoSight NTA 2.3 Analytical Software (Malvern Instruments). For size distributions, nanoparticle concentrations in cell contamination controls for each size class were deducted from the sap samples, providing a correction for the potential contamination of sap with cell debris and cytoplasmic content.

ζ-Potential

ζ-Potentials of nanoparticles in 0.5 mL of freshly expressed xylem sap were measured using a Zetasizer Nano ZS (Malvern Instruments).

ff-EM

Nanoparticles from freshly expressed xylem sap were quenched using the sandwich technique and liquid nitrogen-cooled propane (Papahadjopoulos-Sternberg, 2010). Applying this procedure, a cooling rate of 20,000 K per second is reached, thereby avoiding ice crystal formation and artifacts possibly caused by the cryofixation process. The cryofixed sample was stored in liquid nitrogen for less than 2 h before processing. The fracturing process was carried

out in JEOL JED-9000 freeze-etching equipment where the exposed fracture planes were shadowed with Pt for 30 s at an angle of 25° to 35° and with carbon for 25 s after resetting the specimen angle to 0° (2 kV per 60–70 mA, 1×10^{-5} Torr). The replicas produced this way (Supplemental Fig. S5) were cleaned with concentrated, fuming HNO_3 for 24 h followed by repeating agitation with fresh chloroform:methanol (1:1, v/v) at least five times. The cleaned replicas were examined at a JEOL 100 CX transmission electron microscope, providing a resolution limit of 2 nm for periodic structures.

Supplemental Data

The following supplemental materials are available.

Supplemental Figure S1. Freeze-dried residue from xylem sap of *T. sebifera* in water under phase-contrast light microscopy and fluorescence microscopy.

Supplemental Figure S2. Freeze-dried residue from xylem sap of *G. parviflora* in water under phase-contrast light microscopy and fluorescence microscopy.

Supplemental Figure S3. Freeze-dried residue from xylem sap of *D. buccinatoria* in water under phase-contrast light microscopy and fluorescence microscopy.

Supplemental Figure S4. Freeze-dried residue from xylem sap of *E. farinosa* in water under phase-contrast light microscopy and fluorescence microscopy.

Supplemental Figure S5. The basic steps in freeze-fracture electron microscopy of xylem sap.

Supplemental Movie S1. Nanoparticles (including mainly nanobubbles) in xylem sap freshly extracted from a *G. parviflora* tree on July 14, 2014, in Fullerton, California.

ACKNOWLEDGMENTS

LITERATURE CITED

Abousalham A, Teissere M, Gardies AM, Verger R, Noat G (1995) Phospholipase D from soybean (*Glycine max* L.) suspension-cultured cells: purification, structural and enzymatic properties. Plant Cell Physiol **36:** 989–996

Adams CWM, Bayliss OB (1971) Schiff reactions with lipids and the disputed terminal rinse with hydrochloric acid. Histochemie **28:** 220–224

Amin M (1982) Ascent of sap in plants by means of electrical double layers. J Biol Phys **10:** 103–109

Angeles G, Bond B, Boyer JS, Brodribb T, Brooks JR, Burns MJ, Cavender-Bares J, Clearwater M, Cochard H, Comstock J, et al (2004) The cohesion-tension theory. New Phytol **163:** 451–452

APG III (2009) An update of the Angiosperm Phylogeny Group classification for the orders and families of flowering plants: APG III. Bot J Linn Soc **161:** 105–121

Askenasy E (1895) Ueber das Saftsteigen. Verhandlungen des Naturhistorisch-medizinischen Vereins zu Heidelberg **5:** 325–345

Atchley AA (1989) The Blake threshold of a cavitation nucleus having a radius-dependent surface tension. J Acoust Soc Am **85:** 152–157

Bargmann BOR, Laxalt AM, ter Riet B, Testerink C, Merquiol E, Mosblech A, Leon-Reyes A, Pieterse CMJ, Haring MA, Heilmann I, et al (2009) Reassessing the role of phospholipase D in the *Arabidopsis* wounding response. Plant Cell Environ **32:** 837–850

Blake FG (1949) The Onset of Cavitation in Liquids: Cavitation Threshold Sound Pressures in Water as a Function of Temperature and Hydrostatic Pressure. Acoustics Research Laboratory, Department of Engineering Sciences and Applied Physics, Harvard University, Cambridge, MA

Blander M, Katz JL (1975) Bubble nucleation in liquids. AIChE J **21:** 833–848

Bloch SH, Wan M, Dayton PA, Ferrara KW (2004) Optical observation of lipid- and polymer-shelled ultrasound microbubble contrast agents. Appl Phys Lett **84:** 631–633

Borkent BM, Dammer SM, Schönherr H, Vancso GJ, Lohse D (2007) Superstability of surface nanobubbles. Phys Rev Lett **98:** 204502

Bose JC (1923) The Physiology of the Ascent of Sap. Longmans, Green, London

Brancewicz C, Rasmussen DH, Papahadjopoulos-Sternberg B (2006) Hydrophobic gas bubble formation in Definity: a freeze fracture electron microscopy study. J Dispers Sci Technol **27:** 761–765

Briggs LJ (1950) Limiting negative pressure of water. J Appl Phys **21:** 721–722

Brodersen C, Jansen S, Choat B, Rico C, Pittermann J (2014) Cavitation resistance in seedless vascular plants: the structure and function of interconduit pit membranes. Plant Physiol **165:** 895–904

Brodersen CR, McElrone AJ, Choat B, Lee EF, Shackel KA, Matthews MA (2013) *In vivo* visualizations of drought-induced embolism spread in *Vitis vinifera*. Plant Physiol **161:** 1820–1829

Brodersen CR, McElrone AJ, Choat B, Matthews MA, Shackel KA (2010) The dynamics of embolism repair in xylem: in vivo visualizations using high-resolution computed tomography. Plant Physiol **154:** 1088–1095

Buhtz A, Kolasa A, Arlt K, Walz C, Kehr J (2004) Xylem sap protein composition is conserved among different plant species. Planta **219:** 610–618

Byrne JM (1962) The uptake of dyes by extracted phospholipids and cerebrosides. Q J Microsc Sci **103:** 47–56

Canny MJ (1995) A new theory for the ascent of sap: cohesion supported by tissue pressure. Ann Bot (Lond) **75:** 343–357

Capron M, Tordjeman P, Charru F, Badel E, Cochard H (2014) Gas flow in plant microfluidic networks controlled by capillary valves. Phys Rev E Stat Nonlin Soft Matter Phys **89:** 033019

Caupin F, Cole MW, Balibar S, Treiner J (2008) Absolute limit for the capillary rise of a fluid. EPL **82:** 1–6

Chen IT, Sessoms DA, Sherman Z, Choi E, Vincent O, Stroock AD (2016) Stability limit of water by metastable vapor-liquid equilibrium with nanoporous silicon membranes. J Phys Chem B **120:** 5209–5222

Cho HJ, Mizerak JP, Wang EN (2015) Turning bubbles on and off during boiling using charged surfactants. Nat Commun **6:** 8599

Choat B, Jansen S, Brodribb TJ, Cochard H, Delzon S, Bhaskar R, Bucci SJ, Feild TS, Gleason SM, Hacke UG, et al (2012) Global convergence in the vulnerability of forests to drought. Nature **491:** 752–755

Chomas JE, Dayton P, Allen J, Morgan K, Ferrara KW (2001) Mechanisms of contrast agent destruction. IEEE Trans Ultrason Ferroelectr Freq Control **48:** 232–248

Christensen-Dalsgaard KK, Tyree MT, Mussone PG (2011) Surface tension phenomena in the xylem sap of three diffuse porous temperate tree species. Tree Physiol **31:** 361–368

Cochard H, Hölttä T, Herbette S, Delzon S, Mencuccini M (2009) New insights into the mechanisms of water-stress-induced cavitation in conifers. Plant Physiol **151:** 949–954

Côté WA Jr (1958) Electron microscope studies of pit membrane structure. For Prod J **8:** 296–301

Cox DJ, Thomas JL (2013) Rapid shrinkage of lipid-coated bubbles in pulsed ultrasound. Ultrasound Med Biol **39:** 466–474

Craig VSJ (2011) Very small bubbles at surfaces: the nanobubble puzzle. Soft Matter **7:** 40–48

Crum L (1982) Nucleation and stabilization of microbubbles in liquids. Appl Sci Res **38:** 101–115

Dafoe NJ, Constabel CP (2009) Proteomic analysis of hybrid poplar xylem sap. Phytochemistry **70:** 856–863

Dixon HH (1914a) On the tensile strength of sap. Scientific Proceedings of the Royal Dublin Society **14:** 229–234

Dixon HH (1914b) Transpiration and the Ascent of Sap in Plants. Macmillan, London

Dixon HH, Joly J (1895) On the ascent of sap. Philos Trans R Soc Lond B Biol Sci **186:** 563–576

Dixon MA, Tyree MT (1984) A new stem hygrometer, corrected for temperature gradients and calibrated against the pressure bomb. Plant Cell Environ **7:** 693–697

Djordjevic MA, Oakes M, Li DX, Hwang CH, Hocart CH, Gresshoff PM (2007) The *Glycine max* xylem sap and apoplast proteome. J Proteome Res **6:** 3771–3779

Domec JC (2011) Let's not forget the critical role of surface tension in xylem water relations. Tree Physiol **31:** 359–360

Donaldson LA, Radotic K (2013) Fluorescence lifetime imaging of lignin autofluorescence in normal and compression wood. J Microsc **251:** 178–187

Duncan PB, Needham D (2004) Test of the Epstein-Plesset model for gas microparticle dissolution in aqueous media: effect of surface tension and gas undersaturation in solution. Langmuir **20:** 2567–2578

Dusotoit-Coucaud A, Brunel N, Tixier A, Cochard H, Herbette S (2014) Hydrolase treatments help unravel the function of intervessel pits in xylem hydraulics. Physiol Plant **150:** 388–396

Ellis EA (2014) Staining sectioned biological specimens for transmission electron microscopy: conventional and en bloc stains. *In* J Kuo, ed, Electron Microscopy: Methods and Protocols, Ed 3. Humana Press, New York, pp 57–72

Emory SF (1989) Principles of integrity testing hydrophylic microporous membrane filters, part I. Pharmaceutical Technology **13:** 68–77

Feder N, O'Brien TP (1968) Plant microtechnique: some principles and new methods. Am J Bot **55:** 123–142

Fineran BA (1997) Cyto- and histochemical demonstration of lignins in plant cell walls: an evaluation of the chlorine water ethanolamine silver nitrate method of Coppick and Fowler. Protoplasma **198:** 186–201

Fukuda K, Kawaguchi D, Aihara T, Ogasa MY, Miki NH, Haishi T, Umebayashi T (2015) Vulnerability to cavitation differs between current-year and older xylem: non-destructive observation with a compact magnetic resonance imaging system of two deciduous diffuse-porous species. Plant Cell Environ **38:** 2508–2518

Gartner BL, Moore JR, Gardiner BA (2004) Gas in stems: abundance and potential consequences for tree biomechanics. Tree Physiol **24:** 1239–1250

Goetzman ES, Alcorn JF, Bharathi SS, Uppala R, McHugh KJ, Kosmider B, Chen R, Zuo YY, Beck ME, McKinney RW, et al (2014) Long-chain acyl-CoA dehydrogenase deficiency as a cause of pulmonary surfactant dysfunction. J Biol Chem **289:** 10668–10679

Gonorazky G, Laxalt AM, Dekker HL, Rep M, Munnik T, Testerink C, de la Canal L (2012) Phosphatidylinositol 4-phosphate is associated to extracellular lipoproteic fractions and is detected in tomato apoplastic fluids. Plant Biol (Stuttg) **14:** 41–49

Gortan E, Nardini A, Salleo S, Jansen S (2011) Pit membrane chemistry influences the magnitude of ion-mediated enhancement of xylem hydraulic conductance in four Lauraceae species. Tree Physiol **31:** 48–58

Greenidge KNH (1952) An approach to the study of vessel length in hardwood species. Am J Bot **39:** 570–574

Greenidge KNH (1954) Studies in the physiology of forest trees. I. Physical factors affecting the movement of moisture. Am J Bot **41:** 807–811

Hedges LO, Whitelam S (2012) Patterning a surface so as to speed nucleation from solution. Soft Matter **8:** 8624–8635

Holbrook NM, Burns MJ, Field CB (1995) Negative xylem pressures in plants: a test of the balancing pressure technique. Science **270:** 1193–1194

Hölttä T, Juurola E, Lindfors L, Porcar-Castell A (2012) Cavitation induced by a surfactant leads to a transient release of water stress and subsequent 'run away' embolism in Scots pine (*Pinus sylvestris*) seedlings. J Exp Bot **63:** 1057–1067

Iwai H, Usui M, Hoshino H, Kamada H, Matsunaga T, Kakegawa K, Ishii T, Satoh S (2003) Analysis of sugars in squash xylem sap. Plant Cell Physiol **44:** 582–587

Jansen S, Choat B, Pletsers A (2009) Morphological variation of intervessel pit membranes and implications to xylem function in angiosperms. Am J Bot **96:** 409–419

Jansen S, Schenk HJ (2015) On the ascent of sap in the presence of bubbles. Am J Bot **102:** 1561–1563

Jelínková A, Malínská K, Simon S, Kleine-Vehn J, Parezová M, Pejchar P, Kubeš M, Martinec J, Friml J, Zazímalová E, et al (2010) Probing plant membranes with FM dyes: tracking, dragging or blocking? Plant J **61:** 883–892

Khurana AK, Chen H, Wall CG (1998) Nucleation of gas bubbles in surface irregularities. Chem Eng Commun **165:** 199–215

Kim JS, Daniel G (2013) Developmental localization of homogalacturonan and xyloglucan in pit membranes varies between pit types in two poplar species. IAWA J **34:** 245–262

King MD, Marsh D (1987) Head group and chain length dependence of phospholipid self-assembly studied by spin-label electron spin resonance. Biochemistry **26:** 1224–1231

Klepsch MM, Schmitt M, Knox JP, Jansen S (2016) The chemical identity of intervessel pit membranes in *Acer* challenges hydrogel control of xylem hydraulic conductivity. AoB Plants **8:** plw052

Knipfer T, Brodersen CR, Zedan A, Kluepfel DA, McElrone AJ (2015) Patterns of drought-induced embolism formation and spread in living walnut saplings visualized using x-ray microtomography. Tree Physiol **35:** 744–755

Koch GW, Sillett SC, Jennings GM, Davis SD (2004) The limits to tree height. Nature **428:** 851–854

Kohonen MM (2006) Engineered wettability in tree capillaries. Langmuir **22:** 3148–3153

Kovalenko A, Polavarapu P, Gallani JL, Pourroy G, Waton G, Krafft MP (2014) Super-elastic air/water interfacial films self-assembled from soluble surfactants. ChemPhysChem **15:** 2440–2444

Krishnan HB, Natarajan SS, Bennett JO, Sicher RC (2011) Protein and metabolite composition of xylem sap from field-grown soybeans (*Glycine max*). Planta **233:** 921–931

Kwan JJ, Borden MA (2010) Microbubble dissolution in a multigas environment. Langmuir **26:** 6542–6548

Kwan JJ, Borden MA (2012) Lipid monolayer collapse and microbubble stability. Adv Colloid Interface Sci **183-184:** 82–99

Lamb M, Koch GW, Morgan ER, Shafer MW (2015) A synthetic leaf: the biomimetic potential of graphene oxide. Bioinspiration, Biomimetics, and Bioreplication doi/http://dx.doi.org/10.1117/12.2086567

Laschimke R (1989) Investigation of the wetting behaviour of natural lignin: a contribution to the cohesion theory of water transport in plants. Thermochim Acta **151:** 35–56

Laschimke R, Burger M, Vallen H (2006) Acoustic emission analysis and experiments with physical model systems reveal a peculiar nature of the xylem tension. J Plant Physiol **163:** 996–1007

Lee S, Kim DH, Needham D (2001) Equilibrium and dynamic interfacial tension measurements at microscopic interfaces using a micropipet technique. 2. Dynamics of phospholipid monolayer formation and equilibrium tensions at water-air interface. Langmuir **17:** 5544–5550

Lee SJ, Kim H, Ahn S (2015) Water transport in porous hydrogel structures analogous to leaf mesophyll cells. Microfluid Nanofluidics **18:** 775–784

Lens F, Sperry JS, Christman MA, Choat B, Rabaey D, Jansen S (2011) Testing hypotheses that link wood anatomy to cavitation resistance and hydraulic conductivity in the genus *Acer*. New Phytol **190:** 709–723

Li S, Lens F, Espino S, Karimi Z, Klepsch M, Schenk HJ, Schmitt M, Schuldt B, Jansen S (2016) Intervessel pit membrane thickness as a key determinant of embolism resistance in angiosperm xylem. IAWA J **37:** 152–171

Liese W (2007) Electron microscopy of wood: the pioneering years. Mitteilungen der Bundesforschungsanstalt für Forst- und Holzwirtschaft **223:** 3–12

Ligat L, Lauber E, Albenne C, San Clemente H, Valot B, Zivy M, Pont-Lezica R, Arlat M, Jamet E (2011) Analysis of the xylem sap proteome of *Brassica oleracea* reveals a high content in secreted proteins. Proteomics **11:** 1798–1813

Lohse D, Zhang X (2015) Surface nanobubbles and nanodroplets. Rev Mod Phys **87:** 981–1035

Longo ML, Lozano MM, Borden MA (2009) Physical chemistry of experimental models for lipid shells of medical microbubbles. Bubble Sci Eng Technol **1:** 18–30

Louisnard O, González-García J (2010) Acoustic cavitation. *In* H Feng, G Barbosa-Vanovas, J Weiss, eds, Ultrasound Technologies for Food and Bioprocessing. Springer, New York, pp 13–64

Lubetkin SD (2003) Why is it much easier to nucleate gas bubbles than theory predicts? Langmuir **19:** 2575–2587

McCully M, Canny M, Baker A, Miller C (2014) Some properties of the walls of metaxylem vessels of maize roots, including tests of the wettability of their lumenal wall surfaces. Ann Bot (Lond) **113:** 977–989

Melcher PJ, Zwieniecki MA, Holbrook NM (2003) Vulnerability of xylem vessels to cavitation in sugar maple: scaling from individual vessels to whole branches. Plant Physiol **131:** 1775–1780

Meyra AG, Kuz VA, Zarragoicoechea GJ (2007) Geometrical and physicochemical considerations of the pit membrane in relation to air seeding: the pit membrane as a capillary valve. Tree Physiol 27: 1401–1405

Moebius F, Or D (2012) Interfacial jumps and pressure bursts during fluid displacement in interacting irregular capillaries. J Colloid Interface Sci 377: 406–415

O'Brien TP, Feder N, McCully ME (1964) Polychromatic staining of plant cell walls. Protoplasma 59: 67–73

Oertli JJ (1971) The stability of water under tension in the xylem. Z Pflanzenphysiol 65: 195–209

Or D, Tuller M (2002) Cavitation during desaturation of porous media under tension. Water Resour Res 38: 19-1–19-14

Or D, Tuller M (2003) Reply to comment by N. Kartal Toker, John T. Germaine, and Patricia J. Culligan on "Cavitation during desaturation of porous media under tension." Water Resour Res 39: 1306

Papahadjopoulos-Sternberg B (2010) Freeze-fracture electron microscopy on domains in lipid mono- and bilayer on nano-resolution scale. In V Weissig, ed, Liposomes: Methods and Protocols. Humana Press, New York, pp 333–349

Parra E, Pérez-Gil J (2015) Composition, structure and mechanical properties define performance of pulmonary surfactant membranes and films. Chem Phys Lipids 185: 153–175

Peirce GJ (1936) Are living cells involved in the ascent of sap? Am J Bot 23: 159–162

Pérez-Gil J (2008) Structure of pulmonary surfactant membranes and films: the role of proteins and lipid-protein interactions. Bichim Biophys Acta 1778: 1676–1695

Pesacreta TC, Groom LH, Rials TG (2005) Atomic force microscopy of the intervessel pit membrane in the stem of Sapium sebiferum (Euphorbiaceae). IAWA J 26: 397–426

Pickard WF (1981) The ascent of sap in plants. Prog Biophys Mol Biol 37: 181–229

Plavcová L, Hacke UG (2011) Heterogeneous distribution of pectin epitopes and calcium in different pit types of four angiosperm species. New Phytol 192: 885–897

Pockman WT, Sperry JS, O'Leary JW (1995) Sustained and significant negative water pressure in the xylem. Nature 378: 715–716

Pu G, Borden MA, Longo ML (2006) Collapse and shedding transitions in binary lipid monolayers coating microbubbles. Langmuir 22: 2993–2999

Rasmussen CJ, Gor GY, Neimark AV (2012) Monte Carlo simulation of cavitation in pores with nonwetting defects. Langmuir 28: 4702–4711

Riemersma JC (1968) Osmium tetroxide fixation of lipids for electron microscopy a possible reaction mechanism. Bichim Biophys Acta 152: 718–727

Rioux D, Nicole M, Simard M, Ouellette GB (1998) Immunocytochemical evidence that secretion of pectin occurs during gel (gum) and tylosis formation in trees. Phytopathology 88: 494–505

Ryan WL, Hemmingsen EA (1998) Bubble formation at porous hydrophobic surfaces. J Colloid Interface Sci 197: 101–107

Saveyn H, De Baets B, Thas O, Hole P, Smith J, Van der Meeren P (2010) Accurate particle size distribution determination by nanoparticle tracking analysis based on 2-D Brownian dynamics simulation. J Colloid Interface Sci 352: 593–600

Schaffer K, Wisniewski M (1989) Development of the amorphous layer (protective layer) in xylem parenchyma of CV Golden Delicious apple, CV Loring peach, and willow. Am J Bot 76: 1569–1582

Schenk HJ, Espino S, Visser A, Esser BK (2016) Dissolved atmospheric gas in xylem sap measured with membrane inlet mass spectrometry. Plant Cell Environ 39: 944–950

Schenk HJ, Steppe K, Jansen S (2015) Nanobubbles: a new paradigm for air-seeding in xylem. Trends Plant Sci 20: 199–205

Schmid R (1965) The fine structure of pits in hardwoods. In WA Côté, Jr, ed, Cellular Ultrastructure of Woody Plants. Syracuse University Press, Syracuse, NY, pp 291–304

Schmid R, Machado RD (1968) Pit membranes in hardwoods: fine structure and development. Protoplasma 66: 185–204

Schmitz N, Koch G, Schmitt U, Beeckman H, Koedam N (2008) Intervessel pit structure and histochemistry of two mangrove species as revealed by cellular UV microspectrophotometry and electron microscopy: intraspecific variation and functional significance. Microsc Microanal 14: 387–397

Schneider H, Thurmer F, Zhu JJ, Wistuba N, Gessner P, Lindner K, Herrmann B, Zimmermann G, Hartung W, Bentrup FW, et al (1999) Diurnal changes in xylem pressure of the hydrated resurrection plant Myrothamnus flabellifolia: evidence for lipid bodies in conducting xylem vessels. New Phytol 143: 471–484

Scholander PF, Bradstreet ED, Hemmingsen EA, Hammel HT (1965) Sap pressure in vascular plants: negative hydrostatic pressure can be measured in plants. Science 148: 339–346

Scholz A, Rabaey D, Stein A, Cochard H, Smets E, Jansen S (2013) The evolution and function of vessel and pit characters with respect to cavitation resistance across 10 Prunus species. Tree Physiol 33: 684–694

Schwendener S (1892) Zur Kritik der neuesten Untersuchungen über das Saftsteigen. Mathematische und Naturwissenschaftliche Mittheilungen der Königlich Preussischen Akademie der Wissenschaften 44: 911–946

Sedgewick SA, Trevena DH (1976) An estimate of the ultimate tensile strength of water. J Phys D Appl Phys 9: L203–L205

Sirsi S, Pae C, Oh DKT, Blomback H, Koubaa A, Papahadjopoulos-Sternberg B, Borden M (2009) Lung surfactant microbubbles. Soft Matter 5: 4835–4842

Smith AM (1994) Xylem transport and the negative pressures sustainable by water. Ann Bot (Lond) 74: 647–651

Sperry JS, Perry AH, Sullivan JEM (1991) Pit membrane degradation and air-embolism formation in ageing xylem vessels of Populus tremuloides Michx. J Exp Bot 42: 1399–1406

Sperry JS, Tyree MT (1988) Mechanism of water stress-induced xylem embolism. Plant Physiol 88: 581–587

Steudle E (2001) The cohesion-tension mechanism and the acquisition of water by plant roots. Annu Rev Plant Physiol Plant Mol Biol 52: 847–875

Strasburger E (1893) Ueber das Saftsteigen. Histologische Beiträge V: 1–94

Sukop MC, Or D (2004) Lattice Boltzmann method for modeling liquid-vapor interface configurations in porous media. Water Resour Res 40: W01509

Thomas J, Ingerfeld M, Nair H, Chauhan SS, Collings DA (2013) Pontamine fast scarlet 4B: a new fluorescent dye for visualising cell wall organisation in radiata pine tracheids. Wood Sci Technol 47: 59–75

Tixier A, Herbette S, Jansen S, Capron M, Tordjeman P, Cochard H, Badel E (2014) Modelling the mechanical behaviour of pit membranes in bordered pits with respect to cavitation resistance in angiosperms. Ann Bot (Lond) 114: 325–334

Torres-Ruiz JM, Jansen S, Choat B, McElrone AJ, Cochard H, Brodribb TJ, Badel E, Burlett R, Bouche PS, Brodersen CR, et al (2015) Direct x-ray microtomography observation confirms the induction of embolism upon xylem cutting under tension. Plant Physiol 167: 40–43

Tyree MT, Zimmermann MH (2002) Xylem Structure and the Ascent of Sap, Ed 2. Springer-Verlag, Berlin

Uchida T, Liu S, Enari M, Oshita S, Yamazaki K, Gohara K (2016) Effect of NaCl on the lifetime of micro- and nanobubbles. Nanomaterials (Basel) 6: 31

US EPA Office of Water (2005) Membrane Filtration Guidance Manual. EPA 815-R-06-009. US Environmental Protection Agency, Cincinnati, OH

Ushikubo FY, Furukawa T, Nakagawa R, Enari M, Makino Y, Kawagoe Y, Shiina T, Oshita S (2010) Evidence of the existence and the stability of nano-bubbles in water. Colloids Surf A Physicochem Eng Asp 361: 31–37

Valle RP, Huang CL, Loo JSC, Zuo YY (2014) Increasing hydrophobicity of nanoparticles intensifies lung surfactant film inhibition and particle retention. ACS Sustain Chem Eng 2: 1574–1580

Valle RP, Wu T, Zuo YY (2015) Biophysical influence of airborne carbon nanomaterials on natural pulmonary surfactant. ACS Nano 9: 5413–5421

Vera F, Rivera R, Romero-Maltrana D, Villanueva J (2016) Negative pressures and the first water siphon taller than 10.33 meters. PLoS ONE 11: e0153055

Vincent O, Marmottant P, Quinto-Su PA, Ohl CD (2012) Birth and growth of cavitation bubbles within water under tension confined in a simple synthetic tree. Phys Rev Lett 108: 184502

Wagner HJ, Schneider H, Mimietz S, Wistuba N, Rokitta M, Krohne G, Haase A, Zimmermann U (2000) Xylem conduits of a resurrection plant contain a unique lipid lining and refill following a distinct pattern after desiccation. New Phytol 148: 239–255

Wang C, Zien CA, Afitlhile M, Welti R, Hildebrand DF, Wang X (2000) Involvement of phospholipase D in wound-induced accumulation of jasmonic acid in Arabidopsis. Plant Cell 12: 2237–2246

Weathersby PK, Homer LD, Flynn ET (1982) Homogeneous nucleation of gas bubbles in vivo. J Appl Physiol 53: 940–946

Wei C, Steudle E, Tyree MT, Lintilhac PM (2001) The essentials of direct xylem pressure measurement. Plant Cell Environ 24: 549–555

Westhoff M, Schneider H, Zimmermann D, Mimietz S, Stinzing A, Wegner LH, Kaiser W, Krohne G, Shirley S, Jakob P, et al (2008) The mechanisms of refilling of xylem conduits and bleeding of tall birch during spring. Plant Biol (Stuttg) **10:** 604–623

Wheeler EA (1981) Intervascular pitting in Fraxinus americana. IAWA Bull **2:** 169–174

Wheeler TD, Stroock AD (2008) The transpiration of water at negative pressures in a synthetic tree. Nature **455:** 208–212

Wheeler TD, Stroock AD (2009) Stability limit of liquid water in metastable equilibrium with subsaturated vapors. Langmuir **25:** 7609–7622

Winkel ES, Ceccio SL, Dowling DR, Perlin M (2004) Bubble-size distributions produced by wall injection of air into flowing freshwater, saltwater and surfactant solutions. Exp Fluids **37:** 802–810

Wisniewski M, Davis G (1995) Immunogold localization of pectins and glycoproteins in tissues of peach with reference to deep supercooling. Trees (Berl) **9:** 253–260

Wisniewski M, Davis G, Schafter K (1991) Mediation of deep supercooling of peach and dogwood by enzymatic modifications in cell-wall structure. Planta **184:** 254–260

Yount DE (1997) On the elastic properties of the interfaces that stabilize gas cavitation nuclei. J Colloid Interface Sci **193:** 50–59

Yount DE, Kunkle TD, D'Arrigo JS, Ingle FW, Yeung CM, Beckman EL (1977) Stabilization of gas cavitation nuclei by surface-active compounds. Aviat Space Environ Med **48:** 185–189

Zhang Z, Xin W, Wang S, Zhang X, Dai H, Sun R, Frazier T, Zhang B, Wang Q (2015) Xylem sap in cotton contains proteins that contribute to environmental stress response and cell wall development. Funct Integr Genomics **15:** 17–26

Zimmermann U, Schneider H, Wegner LH, Haase A (2004) Water ascent in tall trees: does evolution of land plants rely on a highly metastable state? New Phytol **162:** 575–615

Zuo YY, Ding M, Bateni A, Hoorfar M, Neumann AW (2004a) Improvement of interfacial tension measurement using a captive bubble in conjunction with axisymmetric drop shape analysis (ADSA). Colloids Surf A Physicochem Eng Asp **250:** 233–246

Zuo YY, Ding M, Li D, Neumann AW (2004b) Further development of axisymmetric drop shape analysis-captive bubble for pulmonary surfactant related studies. Biochim Biophys Acta **1675:** 12–20

Zuo YY, Do C, Neumann AW (2007) Automatic measurement of surface tension from noisy images using a component labeling method. Colloids Surf A Physicochem Eng Asp **299:** 109–116

Zuo YY, Veldhuizen RA, Neumann AW, Petersen NO, Possmayer F (2008) Current perspectives in pulmonary surfactant: inhibition, enhancement and evaluation. Biochim Biophys Acta **1778:** 1947–1977

Zwieniecki MA, Holbrook NM (2000) Bordered pit structure and vessel wall surface properties: implications for embolism repair. Plant Physiol **123:** 1015–1020